Evaluating the MIT S-band coffee can radar as an educational radar

Presented by:
Samuel Kalenga Mbiya

Prepared for:
Dr Yunus Abdul Gaffar
Department of Electrical Engineering
University of Cape Town

Submitted to the Department of Electrical Engineering at the University of Cape Town in partial fulfilment of the academic requirements for a Bachelor of Science degree in Electrical and Computer Engineering

May 30, 2022

Key words: electrical engineering education, radar, inverse synthetic aperture radar imaging

Plagiarism declaration

1. I know that plagiarism is wrong. Plagiarism is to use another's work and pretend that it is one's own.
2. I have used the IEEE convention for citation and referencing. Each contribution to, and quotation in, this report from the work(s) of other people has been attributed, and has been cited and referenced.
3. This report is my own work.
4. I have not allowed, and will not allow, anyone to copy my work with the intention of passing it off as their own work or part thereof.

Signature: .....
S. K. Mbiya

Date: .....
30 May 2022

Abstract

This report aims to describe the evaluation of the MIT S-band coffee can radar as an educational tool. The project came about from the goal of incorporating the radar into the Radar masters course at the University of Cape Town to allow students to collect radar data using a low cost and educational radar. The project was divided into three phases: the first phase involved developing and conducting low frequency subsystem and integration tests to determine whether the radar was functioning correctly. The second phase involved conducting indoor and outdoor experiments to demonstrate the radar's capabilities to measure target range and velocity. The last phase of the project involved designing an Inverse Synthetic Aperture Radar imaging demonstrator using the radar. It was found that the radar system functioned mostly as expected on a subsystem level. The results from the experiments showed that the radar could measure the speed of targets and distinguish between a human target walking, jogging and sprinting. The maximum range of the radar was found to be between 30 - 50 m for human targets. Lastly, the radar was found capable to be utilised for Inverse Synthetic Aperture Radar imaging in the educational context and was able to generate low-resolution images of corner reflector targets. During each phase of the project, it was observed that the radar possessed educational value in terms of electronics, radar applications and system design.

Acknowledgements

This project could not have been complete without the support and encouragement received along the journey.

Firstly, I would to thank the Almighty God for His grace, blessings and the breath of life everyday.

To the Council for Scientific and Industrial Research (CSIR), thank you for your financial support throughout my undergraduate studies and for the numerous opportunities to do vacation work.

To my supervisor, Dr Yunus Abdul Gaffar, thank your for your constant encouragement, support and help during the course of this project. I gained a lot from your knowledge on Radar and have learnt a lot from you as a person.

To the White lab technicians, thank you Brendon and Justin for your assistance in the lab and for storing the radar throughout the project.

To Steve, thank you for assisting me with my radar experiments in the lab. It was a pleasure to work together with you.

To my parents, Laurent and Patricia Mbiya, thank you for your love, support and constant encouragement. Without you as my pillars of strength, I wouldn't be where I am today.

To the Kamonga family, thank you papa José and maman Fofo, for providing me with a "home away from home" during my undergraduate studies in Cape Town. The opportunities I got to be in a family environment helped me a lot to de-stress, when I needed to get away from the stresses of university life.

Nomenclature

RF	Radio Frequency
SAR	Synthetic Aperture Radar
LOS	Line of sight
ISAR	Inverse Synthetic Aperture Radar
Radar	Radio Detection and Ranging
VCO	Voltage Controlled Oscillator
IF	Intermediate Frequency
CW	Continuous Wave
FMCW	Frequency Modulated-Continuous Wave
UCT	University of Cape Town
SNR	Signal-to-noise Ratio
PRF	Pulse Repetition Frequency
PRI	Pulse Repetition Interval

Contents

List of Figures

List of Tables

Chapter 1

Introduction

1.1 Background and problem statement

This research project aimed to contribute to practical-based teaching and learning in the Electrical engineering discipline and the teaching and learning at the University of Cape Town in the field of Radar. The project came about from the goal of incorporating the collection of real-world radar data and radar signal processing in the Radar masters programme at the University of Cape Town. The current coursework, such as in the Fundamentals of Radar Signal and Data Processing course, involves projects where processing is done on existing measured radar datasets or on simulated data. However, the students do not have the opportunity to plan experiments and utilise an educational radar as a tool to gather data from real-world targets.

In the literature, the MIT coffee can radar has been used extensively to measure the range and Doppler frequency of targets [7, 8, 9, 10, 11], and to generate 2-D synthetic aperture radar (SAR) images [12, 13]. However, there is no work on using the radar to generate 2-D inverse synthetic aperture radar (ISAR) images or developing a demonstrator system to learn about ISAR. Therefore, the purpose of this research project was to evaluate the effectiveness of using the MIT coffee can radar as an educational tool to help teach, and learn practical and real-world concepts in Radar, Electronics and Radio frequency engineering and to development of an experimental ISAR demonstrator.

In the process, the goal was also to keep the Radar masters programme in mind by developing test procedures for the radar that could possibly be utilised as a starting point, if the MIT coffee can radar were built and used in the Radar masters programme. This would enable students who utilise the radar for the first time to be able to test the "health" of radar before using it to conduct experiments and to help troubleshoot if any problems arise.

1.2 Objectives

The objectives of the project were to:

- Develop and conduct tests to determine whether the radar was functional on a sub-system level
- Develop and conduct indoor and outdoor experiments to demonstrate the capabilities of the radar
- Develop a prototype system to demonstrate Inverse Synthetic Aperture Radar (ISAR) imaging using the radar

1.3 Original contributions

The MIT coffee can radar has already been widely used in the literature for different purposes such as sensing of range and Doppler frequency [7, 8, 9, 10, 11] and SAR imaging [12, 13]. In Chapter 8, code was written to extend the code written by Charvat et. al [4] for the purposes of Inverse Synthetic Aperture Radar imaging and it was demonstrated that MIT coffee can radar could successfully be utilised for Inverse Synthetic Aperture Radar imaging demonstrations for educational purposes

1.4 Project scope and limitations

In terms of scope, the duration of the project was 13 weeks. The system testing performed on the radar system was limited to only the low frequency electronic circuits. This means that no tests were conducted on the radio frequency (RF) circuits of the radar or the antennas. The testing equipment was also limited to the lab equipment available in White laboratory (undergraduate electronics lab) at the University of Cape Town. The radar system that was evaluated was built by a previous final year undergraduate student.

1.5 Report outline

- Chapter 2 discusses the Radar theory that was relevant to the overall project
- Chapter 3 discusses the theory on Inverse synthetic aperture radar imaging that was relevant to the ISAR imaging prototype design
- Chapter 4 covers the literature review and concludes with a critical review of the literature
- Chapter 5 covers the methodology used to achieve the project objectives.
- Chapter 6 covers the system testing procedures and results
- Chapter 7 covers indoor and outdoor experiments that were performed and their results
- Chapter 8 covers the ISAR demonstrator design
- Chapter 9 discusses the conclusions on the project
- Chapter 10 discusses recommendations for the overall project and potential future work

Chapter 2

Radar theory

This chapter aims to introduce the reader to the radar concept and the main ideas involved in the project.

2.1 The radar concept

Radio Detection and Ranging, also known as Radar, is a sub-field within Radio frequency (RF) engineering which involves making use of radio frequencies (RF) within the electromagnetic spectrum to determine the velocity and position of targets. This involves transmitting RF signals into the environment and then listening for the echoes that are reflected from targets in the environment and returned to the radar. From the frequency and phase information returned in the reflected signals, processing can be applied to the measured data to estimate a target's position and radial velocity.

2.1.1 Radar measurements

Target position

Based on the time delay taken for the echoes to return to the radar after being transmitted, the distance (also known as range) from the radar to the targets can be determined. This depends on the round-trip time delay taken from transmission and reception of the reflected signal. The formula used to calculate the range is given by:

$$R = \frac{c \cdot \tau}{2} \tag{2.1}$$

where R is the range, c is the speed of light in a vacuum, which is approximately $= 3 \cdot 10^8$ m/s and τ is the round-trip time delay. If the azimuth angle, θ and elevation angle, ϕ of the radar is known then a target's position can be estimated in 3-dimensional space as shown in Fig. 2.1 .

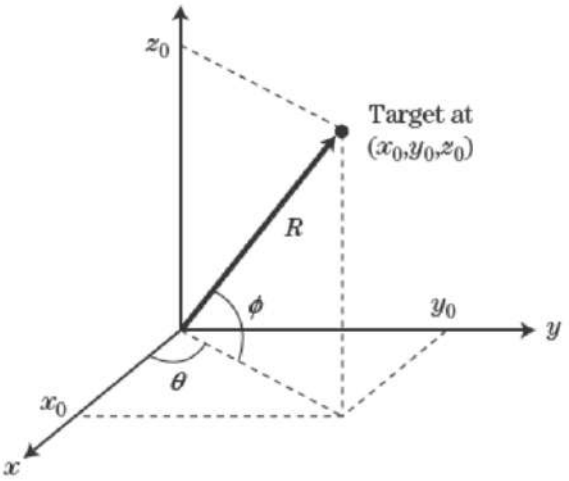

Figure 2.1: An image showing a target's position in 3-dimensional space [1]

Velocity

The reflected signal will have a different frequency than the transmitted signal if a target is in motion relative to the radar. This frequency shift is based on the Doppler effect phenomena. This difference between the transmitted and received frequency is called the Doppler frequency, f_D and it is related to the radial velocity of the target relative to the radar system. The Doppler frequency, f_D is expressed as:

$$f_D = \frac{2 \cdot v_r}{c} \cdot f_t = \frac{2 \cdot v_r}{\lambda_t} \tag{2.2}$$

, where v_r is the radial velocity, f_t is the transmitted frequency, λ_t is the transmitted wavelength and c is the speed of light. Therefore, the radial velocity is given by:

$$v_r = \frac{c}{2 \cdot f_t} f_D \tag{2.3}$$

2.1.2 Resolution

One of the ways to measure the ability or performance of a radar is through the resolution of its measurements. The two common resolutions are the range resolution and Doppler resolution.

Range resolution

The range resolution, ΔR, of a radar determines a radar system's ability to distinguish the range of two closely spaced targets. The range resolution value defines the smallest spacing between two targets that is still distinguishable by the radar and depends on the bandwidth of the transmitted signal. The range resolution is expressed as:

$$\Delta R = \frac{c}{2B} \tag{2.4}$$

, where c is the speed of light and B is the transmitted bandwidth. From this expression, it is clear that a higher bandwidth provides better resolution.

Doppler resolution

The Doppler resolution, Δf, determines the radar system's ability to distinguish between the Doppler frequencies of targets that are moving at similar radial velocities. It depends on the the time duration that the radar beam illuminates the targets. In radar, terminology this is referred to as the dwell or observation time [1]. The Doppler resolution is expressed as

$$\Delta f = \frac{1}{T} \tag{2.5}$$

, where T is the dwell time.

2.2 Radar configurations

There are various radar configurations, however, a simpler configuration to analyse is the homodyne receiver radar configuration [1]. A typical homodyne radar system as shown in Fig. 2.2 is made up of the following components:

- **Antennas**: The transmit and receive antennas are responsible for transmitting the RF signal and receiving the reflected echoes, respectively.
- **Oscillator**: The oscillator, commonly a voltage-controlled oscillator (VCO), is responsible for generating the RF signal to be transmitted. The frequency of the RF signal is set by the voltage provided by the signal generated by the modulator
- **Modulator**: Sets the frequency of the RF signal generated by the oscillator
- **Mixer**: The mixer is responsible for producing an intermediate frequency (IF) signal which contains frequency and phase information on the targets that are in the radar's line of sight (LOS)
- **Low pass filter**: A low pass filter is required to attenuate the unwanted frequencies and mixer products, and to pass through the desired signal, called the baseband signal, without attenuation so that it can be sampled [1].
- **Processor**: In modern radars, processors (or computers) are utilised for applying detection algorithms on the received baseband signal. This allows the characteristics of the target, such as the velocity and range to be estimated.

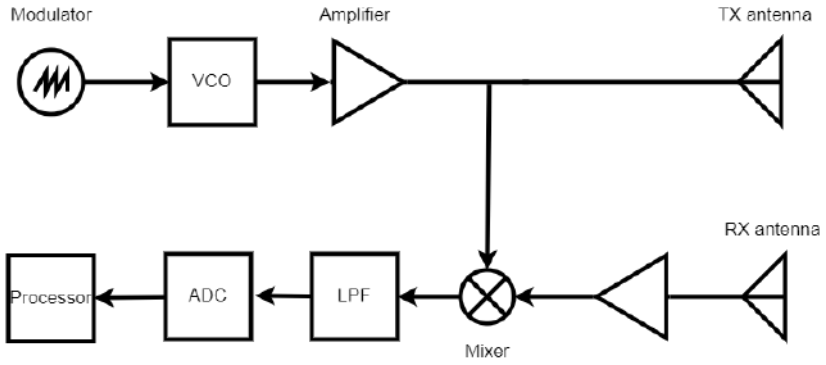

Figure 2.2: A diagram showing the block diagram of a homodyne radar system

Depending on the application of the radar and the target characteristics (range and velocity) that are to be measured different waveforms are transmitted. The two most common waveforms are i) Continuous Wave (CW) waveforms and pulsed waveforms.

2.2.1 Continuous Wave (CW) radars

CW-Doppler radars

CW radars are radars that continuously transmit radio waves at a constant frequency and listen for echoes returned from targets at the same time. CW radars that transmit at a constant frequency are mostly used for measuring the radial velocity of targets. They can do this based on the phenomenon of the Doppler effect. The Doppler effect can be observed when a target is moving because the frequency of the signal that is reflected to the radar will shift from the transmitted frequency, f_t [2]. This difference between the transmitted and received frequency is called the Doppler frequency, f_D, and can be determined by locating the peak frequency in the spectrum of the received signal. As the target moves towards the radar system, the received frequency will increase and the Doppler frequency will increase. From the Doppler frequency, the radial velocity, v_r, of a target can be measured using the equation below:

$$f_d = \frac{2 \cdot v_r}{c} \cdot f_t = \frac{2 \cdot v_r}{\lambda_t} \tag{2.6}$$

The assumption made is that the target's radial velocity is much smaller than the speed of light, c.

Though electromagnetic waves are transmitted by the radar system, the transmitted and received signals can be expressed as sinusoidal signals $S_T(t)$ and $S_R(t)$, respectively. Let the transmitted signal, $S_T(t)$ be expressed as:

$$S_T(t) = A_T cos(2\pi f_T t) \tag{2.7}$$

, where f_T = transmitted frequency

and the received signal, $S_R(t)$ be expressed as:

$$S_R(t) = A_R cos(2\pi f_R t) \tag{2.8}$$

, where f_R = received frequency

If the target is not in motion, the transmitted and received frequency are equal: $f_R = f_T$. However, if the target is in motion toward the radar, a positive Doppler frequency, f_D will be present and $f_R = f_T + f_D$. Therefore, the received signal will then be expressed as:

$$S_R(t) = A_R cos(2\pi(f_T + f_D)t) \tag{2.9}$$

By taking the Fast Fourier Transform of a sampled version of $S_R(t)$, the Doppler frequency and the radial velocity of the target can be determined using the formula:

$$v_r = \frac{c}{2 \cdot f_T} f_D \tag{2.10}$$

CW radars that transmit RF signals of constant frequency are limited in that they cannot measure the range of targets. The fact they are continuously transmitting and listening provides no mechanism to determine the time delay, τ, of the received signal reflected from the targets. To allow range measurement, frequency modulated continuous wave (FMCW) waveforms are transmitted instead.

FMCW radars

FMCW radars are radars that also transmit continuous waves, however, the frequency of the transmitted signals changes over time within a certain bandwidth, B. These signals are called chirps. As mentioned before, range resolution is an important aspect of a radar's ability to distinguish between targets that are close to each other, therefore a large transmit bandwidth is required to achieve this goal. The commonly used modulation waveforms to achieve the varying frequency are the sawtooth and symmetric triangular waveforms, shown in Fig. 2.3.

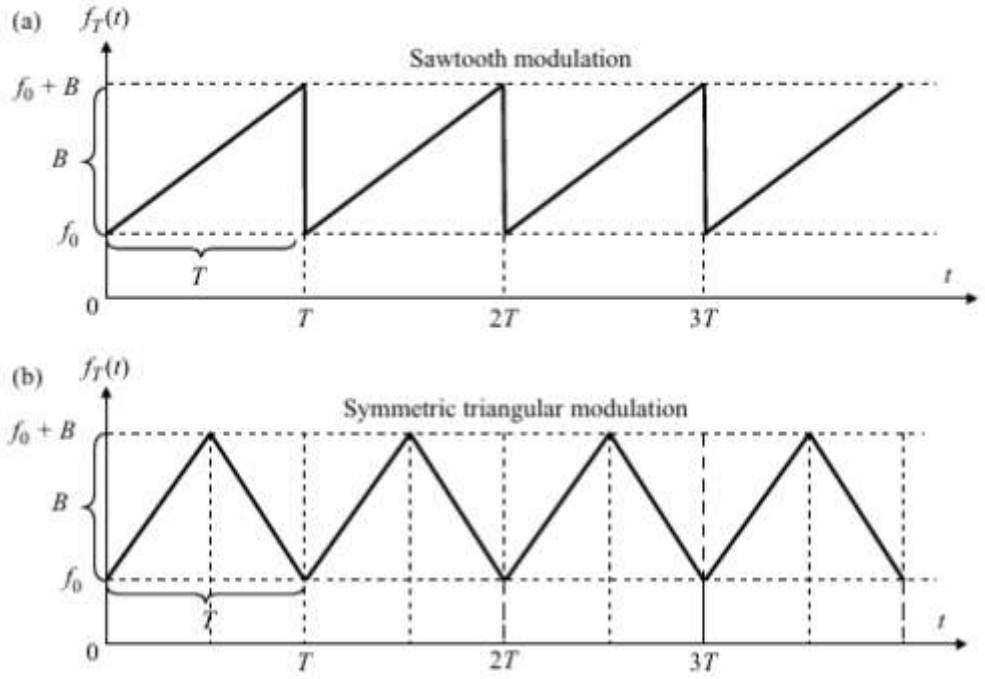

Figure 2.3: An image showing frequency modulation patterns used for FMCW radar [2]

The sawtooth frequency modulation pattern can be mathematically expressed as:

$$f_{sawtooth}(t) = f_0 + \frac{B}{T_c}t \tag{2.11}$$

A triangular frequency modulation pattern can be expressed as:

$$f_{triangular}(t) = \begin{cases} f_0 + \frac{B}{T_c}t, (0 \leq t \leq T_c) \\ f_0 + B - \frac{B}{T_c}(t - T_c), (T_c \leq t \leq T) \end{cases} \tag{2.12}$$

, where f_0 is the starting frequency, B is the frequency bandwidth and T is the period.

A transmitted signal with a varying frequency over time, $f_T(t)$ can be expressed as:

$$S_T(t) = A_T cos(2\pi f_T(t)) \tag{2.13}$$

If the triangular wave is used to modulate the frequency and only the up-chirp period is considered then the transmitted signal is expressed as:

$$S_T(t) = A_T cos(2\pi f_T(t)t) \tag{2.14}$$
$$= A_T cos(2\pi(f_0 + \frac{B}{T_c}t)t) \tag{2.15}$$
$$= A_T cos(2\pi(f_0 t + \frac{B}{T_c}t^2)) \tag{2.16}$$

The received signal reflected by the target can be expressed as:

$$S_R(t) = A_T cos(2\pi f_T(t)(t-\tau)) \tag{2.17}$$
$$= A_T cos(2\pi(f_0 + \frac{B}{T_c}t)(t-\tau)) \tag{2.18}$$
$$= A_T cos(2\pi(f_0(t-\tau) + \frac{B}{T_c}(t-\tau)^2)) \tag{2.19}$$

, where τ is the round-trip time delay taken for the transmitted signal to be reflected back to the radar system

Once $S_R(t)$ is received it goes through a mixer and the output of the mixer is a signal called the intermediate frequency (IF) signal which contains frequency components that are the sum and difference of $f_T(t)$ and $f_R(t)$. When measuring the range of a target using an FMCW radar, the difference between $f_T(t)$ and $f_R(t)$, called the beat frequency, f_B, is of interest. This is expressed below:

$$f_B = f_T(t) - f_R(t) \tag{2.20}$$
$$= f_0 + \frac{B}{T_c}t - ((f_0 + \frac{B}{T_c}t)(t-\tau)) \tag{2.21}$$
$$= \frac{B}{T_c}\tau \tag{2.22}$$

, where T_c is the up-chirp transmission period, B is the frequency bandwidth of the transmitted signal

Using the relationship between range and round-trip time delay ($\tau = \frac{2R}{c}$), the beat frequency can be expressed as:

$$f_B = \frac{2SR}{c} \tag{2.23}$$

, where S = $\frac{B}{T_c}$

2.2.2 Pulsed radars

Pulsed radars work by firstly transmitting radio waves (pulses) for a short period of time and then switch on their receiver to listen for echoes before the next pulse is transmitted. This means that they transmit pulse-modulated chirp signals. Pulsed radars differ from CW radars because they do not continuously transmit and listen. A pulsed waveform is shown in Fig. 2.4. The performance of pulsed radars depends on their pulse repetition frequency (PRF) and pulse repetitiion interval, which affect the radars unambiguous range and Doppler measurements. The PRF and PRI are related to each other by 2.24,

$$PRI = \frac{1}{PRF} \tag{2.24}$$

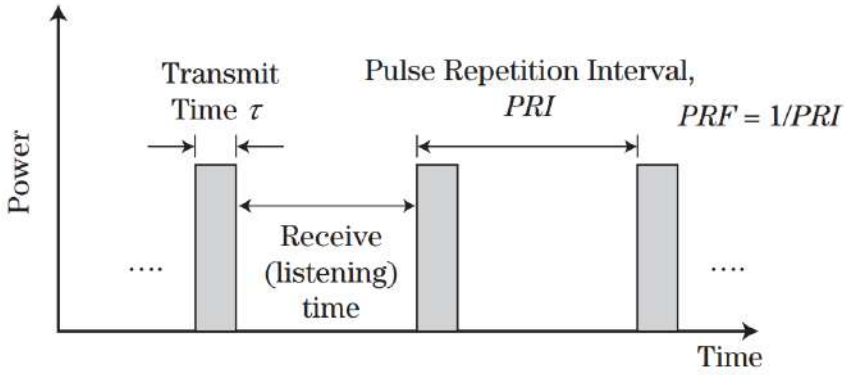

Figure 2.4: An image showing a pulsed waveform [1]

Unambiguous range and Doppler measurement

The maximum range, R_{max}, of a pulsed radar depends on its PRF, expressed in 2.25.

$$R_{max} = \frac{c}{2PRF} \tag{2.25}$$

The maximum Doppler frequency that can be measured, f_{Dmax}, expressed in 2.26, also depends on the PRF.

$$f_{Dmax} = \pm\frac{PRF}{2} \tag{2.26}$$

Therefore, it can be observed that a trade-off needs to be made between range measurement performance and velocity measurement performance.

Chapter 3

Inverse Synthetic Aperture Radar imaging theory

This chapter covers theory related to Inverse Synthetic Aperture Radar (ISAR) imaging that is relevant for the design of the ISAR imaging demonstrator.

3.1 ISAR imaging concept

3.1.1 ISAR comparison to SAR

Synthetic Aperture Radar (SAR) imaging works based on the same radar principle of transmitting a signal and then listening for the echoes that are reflected back from the targets. Images are formed by processing the received signals from different viewing angles of the target and can be interpreted as the 2-Dimensional map of the reflectivity of the target scene [2]. However, with SAR imaging, instead of using large antennas to intercept the reflected signals, a collection of smaller apertures are used to form a larger aperture. The large aperture is usually formed by attaching the radar to a moving platform such as an aircraft. SAR imaging radars can be operated in two different modes, namely, i) strip-map mode and ii) spotlight mode. Strip-map mode is commonly used for generating wide-area maps of terrains by combining the strip maps produced from different areas over the length of the synthetic aperture. Spotlight mode involves focusing the radar beam over the same area over different view angles along the length of the synthetic aperture and is used for generating images of smaller area maps. ISAR imaging is related to a variation of spotlight mode, called circular SAR imaging, which involves the radar platform moving in a circular path around the target area instead of a linear path. However, instead of having a moving radar platform, ISAR imaging involves fixing the position of the radar and allowing the target to move, such as placing the target on a flat rotating platform.

3.1.2 ISAR system model

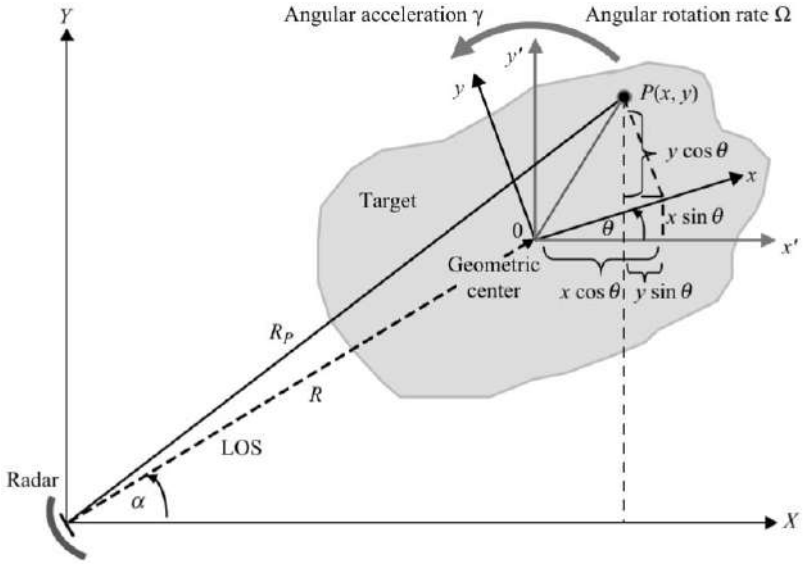

Figure 3.1: An image showing the ISAR system model [2]

ISAR imaging makes use of the rotational motion of a target to generate images. Every target can be considered as a collection of rotating point scatterers, each with its own reflectivity properties, ρ and velocity relative to the radar system, which is dependent on the angular velocity, Ω, of the rotating platform and the distance from the centre of rotation [2]. Every point scatterer, P, on the target reflects a signal to the radar, and it is from the time delay of this reflected signal that its range, R_P can be determined. The signal reflected can be expressed as:

$$\begin{aligned} S_P(t) &= \rho(x,y)e^{-j2\pi f\tau} \\ &= \rho(x,y)e^{-j2\pi f\frac{(2R_P(t))}{c}} \\ &= \rho(x,y)e^{j\frac{4\pi f R_P(t)}{c}} \end{aligned} \tag{3.1}$$

In the same way, each point scatterer also has an associated Doppler frequency, due the velocity caused by the rotation. This can be expressed as:

$$\begin{aligned} f_D(t) &= \frac{2v_r(t)}{c}f_t \\ &= \frac{2v_r(t)}{\lambda_t} \\ &= \frac{2}{\lambda_t}\frac{dR_P(t)}{dt} \end{aligned} \tag{3.2}$$

Therefore, the total signal returned to the radar involves integrating over each signal returned by the point scatterers and is expressed as:

$$S_R(t) = \iint_{-\infty}^{+\infty} \rho(x,y) e^{-j\frac{4\pi f R_P(t)}{c}} dxdy \tag{3.3}$$

3.1.3 ISAR imaging process

The ISAR imaging process can be sub-divided into two stages:

- Transmission and data acquisition
- Data processing and image reconstruction

The entire process from data acquisition to image reconstruction can be summarised in Fig 3.2.

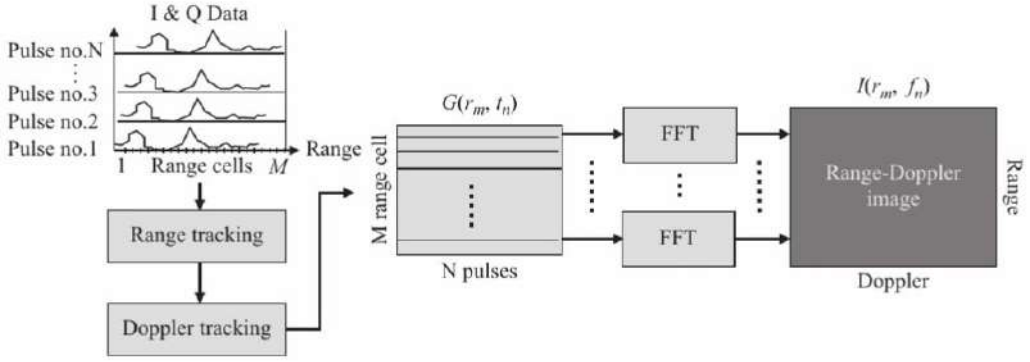

Figure 3.2: An image showing the ISAR imaging process [2]

Transmission and data acquisition

During this stage, the radar transmits a series of pulses and the IF signals produced by mixing the received and transmitted signals are sampled. The sampled signals are then stored in an NxM matrix, where N is the number of pulses transmitted and M is the time samples collected. The time samples associated with each pulse are then processed by performing a Fourier Transform to generate range profiles, which are related to the time delay of the different backscatters. These are arranged in different range bins. When utilising a homodyne FMCW radar, the range of a target would be related to a beat frequency, f_b, (also known as IF) as expressed below

$$R = \frac{c}{2S} f_b \tag{3.4}$$

, where

$c =$ speed of light $(3 \cdot 10^8 m/s)$

$S =$ the change in frequency over time

$R =$ the range measurement in meters

Algorithms such as the Moving Target Indicator (MTI) may also be utilised to reject clutter and stationary targets so that moving targets can be distinguished in the range profiles [1].

Data processing and image reconstruction

Once the range profiles are acquired, they are then further processed for image reconstruction. Generally, the rotational motion of the point scatterers on the target translate to motion in the range profiles. However, if images without blurring or smearing are to be generated, some form of range alignment would need to occur to compensate for the motion. Range alignment algorithms aim to minimise the migration of range profiles between different range bins within the dwell time of the radar. One way to avoid having to apply range alignment algorithms is to minimise the migration of scatterers through the range bins over the dwell time. This can be achieved by considering a very short observation window.

Once the range profiles, a Range-Doppler map can be generated. This involves taking the Fourier Transform at each range bin, across all the pulses considered in the observation window. The Range-Doppler map is essentially the image of the target and is a function of the reflectivity of different point scatterers on the target.

3.2 ISAR image resolution

3.2.1 Range resolution

As mentioned in the radar theory section, one way to measure the performance of a radar is by its range resolution, Δr, given by equation 3.5. The larger the transmit bandwidth, B, the better the resolution.

$$\Delta r = \frac{c}{2B} \tag{3.5}$$

This principle still holds in determining the resolution or quality of the ISAR images produced. A smaller range resolution makes it possible to distinguish between two closely spaced scatterers in an image.

3.2.2 Doppler resolution

Another aspect which determines the quality of an ISAR image is the Doppler resolution, Δf_D . This determines the ability of the radar system to distinguish between the Doppler frequencies of targets that are close to each other. It is expressed as:

$$\Delta f_D = \frac{1}{T} \tag{3.6}$$

, where T is the observation window in seconds.

The observation window is related to the PRI and number of pulses, N by:

$$T = N \cdot PRI \tag{3.7}$$

Therefore, Equation 3.6 can be written as:

$$\Delta f_D = \frac{1}{N \cdot PRI} \tag{3.8}$$

The cross-range resolution , Δr_{cr}, determines a radar's ability to distinguish between two closely spaced target and is related to the Doppler resolution and can be obtained using the relationship:

$$\begin{aligned} f_D &= \frac{2v_r}{\lambda_t} \\ f_D &= \frac{2\Omega r}{\lambda_t} \\ \Delta f_D &= \frac{2\Omega \Delta r_{cr}}{\lambda_t} \end{aligned} \tag{3.9}$$

Therefore, the cross-range resolution, Δr_{cr}, is expressed as

$$\Delta r_{cr} = \frac{\lambda_t}{2\Omega T} \tag{3.10}$$

Chapter 4

Literature Review

This chapter aims to discuss different literature that was related to the project, starting broadly with literature related to Radio frequency engineering education and then funnelling down into different radar systems and their uses. The project contributes to electrical engineering education, specifically in the field of radio frequency (RF) engineering, therefore the literature review starts off by surveying different educational tools that other authors have developed and used to teach concepts in RF engineering at universities. The project focuses on evaluating a radar system, therefore a survey on commercially available radar kits was conducted to see their capabilities and features and to see if there are any kits that have the potential to be used for educational purposes. In the last two sections, an overview of the original MIT S-band coffee can radar's purpose, design and uses are mentioned. The literature review then looks at how other authors have used the MIT S-band coffee can design and the modifications that have been made to the system for different applications. The chapter concludes with a critical review of insights gained, trends and gaps in the literature that is relevant to the project.

4.1 Radio frequency engineering tools used in universities

In [14], Jensen et. al designed a microwave course with laboratory projects to introduce students to component and system-level design and expose them to modern computer-aided design (CAD) tools, microstrip and surface mount fabrication technologies, and industry-standard test equipment and procedures. This was achieved by allowing students to build different sub-systems that would form part of a C-band radar system to i) measure the range of corner reflectors and speed and ii) develop SAR images. For the Doppler experiments, students were tasked to design a 3-dB power splitter and microstrip patch array antenna and the for the SAR imaging, students were tasked with designing and constructing the Wilkinson power dividers, branch-line couplers and bandpass filters implemented on microstrip coupled line filters. The course resulted in increased student enrollments in the subsequent offering and generated more enthusiasm and curiosity amongst the students about the phenomena observed in the laboratory. This also caused the students to be more motivated to tackle the difficult theoretical and physical concepts encountered in the course.

In [15], Camps et. al also present a system engineering course aimed at teaching students about the fundamentals and applications of radio ranging and radio navigation systems. The involved practical work where data had to be collected and processed using demonstration kits in the form a Sonar kit and a GPS-based software program to learn about navigation. In this case, the students were not required to build the sonar kit, but rather used the kits available purely for data collection purposes.

In [16], antenna arrays were used to teach students about antenna theory and sinusoidal signals and their properties. To demonstrate the concept of phase shift, a set of patch antennas were built and different phase shifts were achieved by adding meander (delay) lines to the transmission line of the antennas.

Later in the course, students also built their own antennas using soup cans, called "Cantennas" and had the opportunity to measure the radiation patterns of their antennas. To measure the effectiveness of this approach in the classroom, the authors set up a test for the students after their antenna demonstrations. The outcome of the test showed a noticeable improvement and the authors mentioned that the number of students who stayed behind to ask questions after lectures increased and that it caused an increase in the interest and curiosity of students in the field of electromagnetics.

In [17] the authors describe a microwave circuit design course in which they added laboratory projects around a 5.8 GHz CW Doppler radar experiment board that was developed for the course. The experiment boards were designed in such a way that they could make use of microwave components that the students would build in their laboratory sessions. The final iteration of the experiment board had ports that could accommodate student-designed components, such as a mixer, a 10 dB coupler and antennas, such as the "Cantennas" that are also mentioned in [16]. The students taking the course felt that the use of the radar aided them in practically seeing the applications of the microwave theories that they learnt in class and how the different microwave components work together for the functioning of the whole system. One student even mentioned how a job interviewer was impressed after the student described the coursework that was done in the course.

In [18], the Aydin et. al used a blended laboratory approach, by including a remote radio laboratory to help students learn about the design of the RF and Microwave systems. In addition to physical laboratory sessions where demonstrations took place, students were also required to conduct remote laboratory experiments via a web-based learning tool. The goal of the tool was to help gain fundamental knowledge in electromagnetic wave propagation concepts and how different RF measurement devices work, such as vector network analyzers. Computer-Aided Design (CAD) experiments were added where students used the AWR Design environment to design RC filters, perform analysis on transmission lines and design components such as T-attenuators. Lastly, the students also had the opportunity to design and fabricate their own RF microwave filters. The addition of remote laboratory exercises and CAD helped students gain a good understanding of component design, fabrication and measurement. Many students noted that this course structure made the theoretical concepts make more practical sense.

In [4], a short course on radar was offered to increase the interest of students in the field of applied electromagnetics. In the course, students learned about radar and system-level RF system design. This was achieved mainly by allowing the students to build their own low-cost radar system that was designed for the purpose of the course. The radar design involved substituting traditional antennas for tin coffee cans or "Cantennas". It only required 12 V of power through the use of AA batteries and made use of off-the-shelf RF coaxial components and low frequency analogue circuitry built on breadboards. The students were also able to conduct experiments on ranging, doppler and Synthetic Aperture Radar imaging with the radar system. This same radar system design was also utilised in [19], by Hernandez-Jayo et. al, from the University of Deusto in Spain, who offered a master's course in communications systems.

In [20], a short course was taught on phased array radars during the Independent Activities Period (IAP) at MIT. The purpose of the course was to give students hands-on experience by building a phased array radar. The students were taught concepts such as Time Domain Multiplexed-Multiple Input Multiple

Output (TDM-MIMO).

In [21], Vincent et. al from ENSICA in France describe a low-cost demonstration kit that was developed to teach students about SAR imaging. The demonstrator was constructed as a scale model of a Side-Looking Airborne Radar (SLAR), using a metallic rail and placing the radar on rollers. The radar operated at a carrier frequency of 40 kHz and a frequency bandwidth of 4 kHz.

4.2 Commercially available radar kits

Universal Radar (uRAD)

The uRAD is a set of multipurpose radar kits designed and manufactured by a company called Anteral in Spain [22]. They manufacture radars that operate at 24 GHz, 60 GHz and 77 GHz to measure target position (range and angle), velocity and signal-to-noise ratio (SNR). They offer two tiers of radar systems: basic radar kits and high-performance radar kits.

Basic FMCW radar kit

The basic radar kit, shown in Fig. 4.1 costs 199 Euros and is an FMCW radar that operates at a frequency of 24 GHz and can operate in both CW-Doppler and FMCW mode. It can measure target range only, velocity and SNR. They also provide compatible shields/expansion boards for the Arduino Uno, Raspberry Pi and cross-platform support via USB-UART for smart mobile devices and computers.

Figure 4.1: An image showing basic uRAD FMCW radar expansions boards compatible with the Arduino Uno, Raspberry Pi and USB UART interfaces [3]

Each board requires a supply voltage of 5 V. The radar system makes use of 4x4 patch antenna arrays with a gain of 16.6 dB, an output power of 18 dBm and a beamwidth of 30 degrees in both the azimuth and elevation. The radar has a range resolution of 1.5 m and can achieve a maximum range of 100 m. The velocity resolution is $\pm$ 3 m/s and can measure velocities up to $\pm$ 75 m/s. Each board has average dimensions of 50 x 70 mm and weighs 13 grams. The radars support different frequency modulation patterns such as CW, sawtooth, triangular and dual rate. Each board comes bundled with a program with a graphical user interface (GUI) and the necessary Arduino or Python libraries, allowing the radars

to monitor in real-time, configured and controlled.[23, 24, 25]

High-performance kit

The high-performance kits shown in Fig. 4.2, come in two variants, the industrial uRAD and automotive uRAD, which have a starting cost of 225 Euros and 250 Euros respectively.

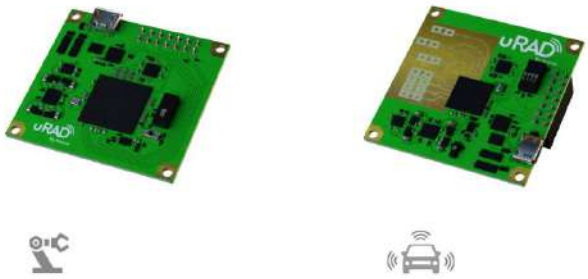

Figure 4.2: An image showing high performance uRAD FMCW radar circuit boards used for industrial (left) and automotive applications (right) [3]

The industrial uRAD is an FMCW radar that operates at a centre frequency between 60-64 GHz. It is mainly used for velocity measurement and 3D positioning of multiple targets. It requires a supply voltage of 5V and has several interfaces, such as a USB and serial port and a Raspberry Pi adaptor. The radar has an antenna beamwidth of 160 degrees in both the azimuth and elevation and has 15 dBm of transmission power. The radar has a range resolution of 5 cm and can achieve a maximum range of up to 70 m for cars and 40 m for human targets. The velocity resolution is ± 0.06 m/s and can measure velocities up to ± 45 m/s. Each radar weighs 5 grams and has dimensions of 42 x 45 x 10 mm.[26]

The automotive uRAD is also an FMCW radar, however, it operates at a centre frequency between 76 - 81 GHz. It is also mainly used for velocity measurement and 3D positioning of multiple targets. It requires a supply voltage of 5 V and has 19 dBm of transmission power. The radar has an antenna beam width of 120 degrees in the azimuth and 40 degrees elevation, making its radiated beam pattern narrower. The radar has a range resolution of 5 cm and can also achieve a maximum range of up to 70 m for cars and 40 m for human targets. The velocity resolution is ± 0.06 m/s and can measure velocities up to ± 45 m/s. Each radar weighs 5 grams and has dimensions of 42 x 45 x 10 mm, similarly to the industrial uRAD. It also supports various interfaces and has a USB, serial port and Raspberry Pi adaptor onboard.[27]

P440 Ultra Wide Band (UWB) radar

The P440 Ultra Wide Band (UWB) radar, shown in Fig. 4.3, is a coherent pulsed radar manufactured by a company called TDSR in the United States of America (USA). This particular radar forms part of a number of Radar kits also developed by the same company. The radar can be used for range measurements between two or more other P440 transceivers and as a general radar. The P440 has an

operating frequency of 3.1 to 4.8 GHz. It requires a supply voltage of at least 4.8 V and consumes up to 2 W of power. The radar's maximum range in a clear line of sight (LOS) is between 300 m to 1.1 km, dependent on the type of antenna height, with an accuracy of up to 2 cm. The radar can produce a PRF up to 125 kHz and supports different interfaces such as Ethernet, USB, Serial, SPI and CAN. Each radar has dimensions of 89 x 56 mm. Each module can be interfaced with via the RangeNet and Monostatic Radar Module (MRM) application programming interfaces (APIs) and graphical user interfaces (GUIs), developed by TDSR. [28]

Figure 4.3: An image showing the P440 Ultra Wide Band pulsed radar

Acconeer XE132

The Acconeer XE132 is a pulsed coherent radar evaluation board manufactured by a company named Acconneer. The radar operates at a centre frequency of 60 GHz and its main applications are low power distance measurements, level measurement, parking space occupancy detection and smart motion detection. The radar requires a supply voltage of 1.8 to 3.6 V and has a power consumption of less than 0.05 mW. The radar has a half-power beamwidth of 40 degrees in the azimuth and 80 degrees in elevation. Depending on the target object and application, the radar can achieve a maximum range between 0.5 - 10m. Additionally, the radar support multiple interfaces as well, such as UART, I2C and GPIO and has dimensions of 25 x 20 mm.[29]

Figure 4.4: An image showing the Acconeer XE132 pulsed radar evaluation board

QM-RDKIT Radar Demonstration Kit

The QM-RDKIT Radar Demonstration Kit developed by Quonset Microwave[30] consists of a radar that has an operating frequency between 2.4 GHz to 2.5 GHz. The radar supports two modes of operation: CW-Doppler and FMCW mode and requires a supply voltage of at least 5 V, which can be provided via a

USB connection to a computer or a battery pack. Additionally, the radar also supports the utilisation of multiple frequency modulation waveforms, such as a single tone for CW mode and it provides the ability to use a ramp and sawtooth waveform for FMCW mode. Though the radar is very similar in terms of specifications and appearance to the PEM11000-KIT radar demonstration kit developed by [31], it only costs 899.99 US Dollars, while the PEM11000-KIT costs almost 3000 US Dollars for one unit.

(a) QM-RDKIT radar[32] (b) PEM1100-KIT radar[33]

Figure 4.5: Images showing the (a) QM-RDKIT S-band FMCW radar and (b) PEM1100-KIT S-band radar

4.3 MIT S-band coffee can radar

The MIT Coffee can radar kit, shown in Fig. 4.6 was developed in 2011 by Charvat et. al[4], for a short course on Radar sponsored by the Lincoln Laboratory at the Massachusetts Institute of Technology (MIT). The course content included concepts such as:

- Applied electromagnetics
- Radio Frequency (RF) engineering design
- Digital Signal Processing
- Analogue circuit design
- Radar system design

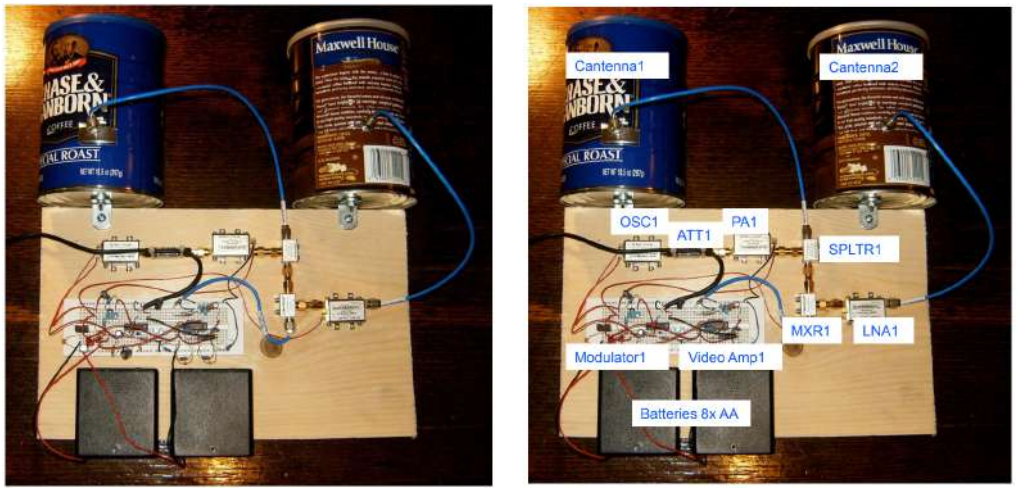

(a) (b)

Figure 4.6: Images showing a top down view of the MIT coffee can radar [4, 5]

The main goal of the course was to allow students to get practical experience by building a low-cost radar project that would involve theory from their physics, electrical and computer engineering courses, and increase their interest in the field of Radar by exposing them to the "big picture" of Radio Frequency engineering. Students who took the course were also able to use the radar system to take measurements of range and velocity. They were also able to to perform SAR imaging with the radar.

System description

The radar kit costs $ 360 and operates in the S-band frequency band defined by the Institute of Electrical and Electronics Engineers (IEEE). It transmits signals with a centre frequency of 2.4 GHz. The radar system requires a supply voltage of 12 V and has a transmission power of almost 10 mW. It consists of three main sub-systems, namely the Radio Frequency (RF) circuit, Low Frequency (LF) circuits and the digital signal processing subsystem. The radar can operate in two modes, as a CW-Doppler radar and an FMCW radar, allowing the measurement of target range (up to almost 1 km at 10 dBsm) and target velocity. The radar can also be utilised for SAR imaging. The radar system design can be considered an "open-source hardware" design because there are available resources on its bill of materials and construction that have been made publicly available online, on the MIT Open Courseware (OCW) website [5].

Radio frequency circuit design

The Radio frequency circuit is made up of a voltage-controlled oscillator (VCO), mixer, splitter, power amplifiers and antennas. Most of the circuits in the RF subsystem were achieved using off-the-shelf coaxial components constructed by Mini-Circuits, except the antennas, which utilised two metal coffee cans as circular waveguides as a low-cost alternative.

Antenna design

The radar system transmits linearly polarised electromagnetic waves by means of its low-cost antennas called "Cantennas". The antennas makes use of coffee cans as circular waveguides, which are 14 cm in length and 9.9 cm in diameter. A quarter wavelength monopole is used and is located 4.6 cm away from the back wall of the waveguide. The antennas achieve a peak gain of 7.2 dBi and a half-power beamwidth of 72 °, shown in Fig. 4.8.

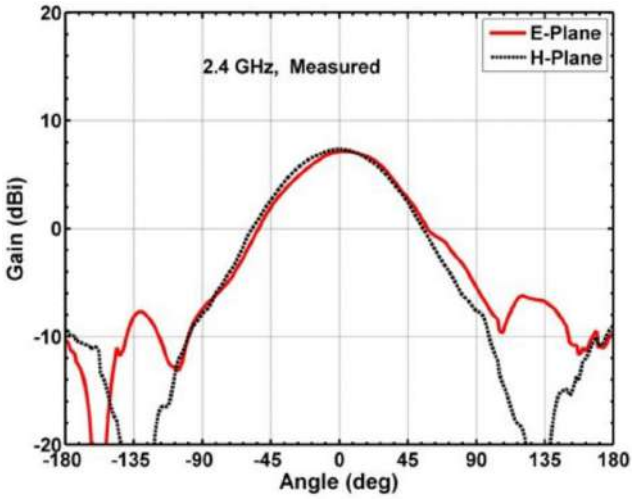

Figure 4.7: A plot showing the gain pattern of the MIT coffee can radar's antennas [4]

Figure 4.8: An image showing the circular waveguide, also known as a "Cantenna" used for the MIT coffee can radar [5]

Radio frequency (RF) Transceiver design

The RF transceiving circuit makes use of the off-the-shelf RF components manufactured by a called Mini-Circuits. It consists of a voltage-controlled oscillator (VCO), frequency mixer, splitter and power amplifiers.

Low frequency (LF) circuit design

The main purpose of LF circuit is to modulate and filter the received signals. The original circuit consists of a modulator circuit and video amplifier built on a breadboard. The modulator circuit is responsible for generating different waveforms required for the operation of the radar, such as the tuning voltage that controls the oscillator, allowing it to produce a linear frequency modulated RF signal. The video amplifier is responsible for filtering out the high frequency components in the received RF signal to produce a baseband signal with a bandwidth limited to the audio frequency range (20 Hz - 20 kHz). This signal is output from the LF circuit through an audio jack cable that can be input into a computer for further processing.

Digital signal processing system

The digital signal processing system is responsible for sampling the filtered baseband signal produced by the frequency mixer and then applying different signal processing algorithms on it, to retrieve range and Doppler frequency information from targets. This system is achieved through the use of a computer and digital audio software to record measurements and the radar signal processing is implemented in software written in Matlab code.

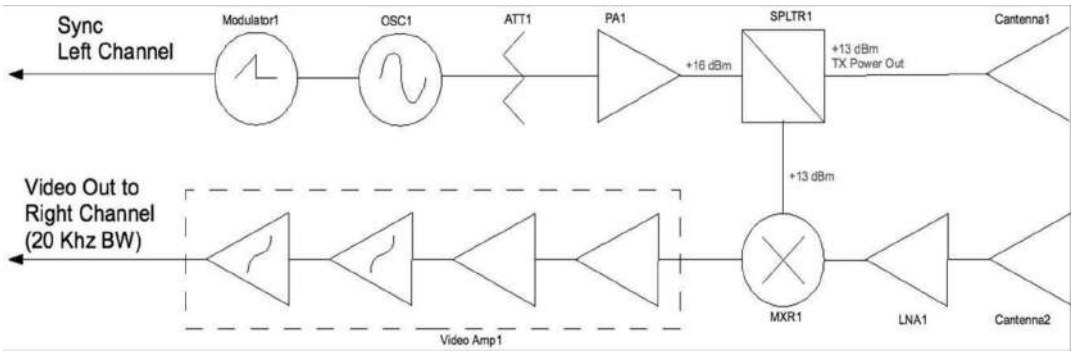

Figure 4.9: An image showing a system block diagram of the MIT coffee can radar system [4]

4.4 Modifications and uses of the MIT S-band coffee can radar

In [12], the design was used for SAR imaging for the purpose of near and very near range analysis. Corner reflectors were used as targets in the scene and it involved placing the radar on a linear rail and capturing recordings as it is moved to different positions along the rail. In terms of modifications, the authors fabricated the low frequency circuit onto a printed circuit board and used patch (planar) antennas instead of the coffee can antennas.

In [7], the radar design was used for measuring velocity and the range of vehicles. In terms of modifications, the authors worked on a redesign in the three main ways, by embedding the signal processing, fabricating the modulation and power sub-system onto a single printed circuit board and a user-friendly interface. For

the embedded processing system a dsPIC microcontroller, which is a specialised digital signal processing (DSP) microcontroller, was utilised to process the IF signal. The microcontroller was also utilised for generating the tuning voltage of the voltage-controlled oscillator (VCO), allowing modulation patterns to be generated and used. The authors did not present any findings from using different modulation patterns. For the power system, instead of using AA batteries similar to [4], the authors designed the system to make use of rechargeable lithium-ion batteries. A battery charger and power selector were designed, to allow the battery to charge up and to allow the system to still be able to run off an external 12 V power supply if required. Circuits for voltage regulation and circuit protection were also designed. An LCD display was used to display the measured speed of vehicles in real-time to users.

In [8], the radar was used for moving target detection and its performance was also compared to the QM-RDKIT radar demonstration kit. Humans and vehicle targets were used for the range and Doppler experiments. The only modifications done to the system were on the antennas, hexahedral phased array antennas were utilised instead of Cantennas.

In [9], the authors proposed modifications to the MIT coffee can radar to make it cheaper, smaller and more performant. The redesign made use of modern RF and EDA design and was tested using range and Doppler simulations. For the antennas, Vivaldi planar antennas printed on a circuit board were used due to their good broadband characteristics, high gain, good impedance matching and manufacturability on a large scale. For the RF sub-system, instead of using off-the-shelf blocks, surface mount components were used to implement the same functionality. The low frequency circuit was also redesigned using parasitic components, such as capacitors and resistors to implement circuits such as the low pass filter and attenuator used in the RF circuit. In terms of the results of the redesign, it provided a +10 dBm improvement in gain and saved $ 110 on the overall costs per system in contrast to the MIT design.

In [13], the radar system was utilised for SAR imaging and an analysis into whether the system could be used on mini-UAVs was performed. A sports court was used as the target scene for the imaging and targets such as trihedral corner reflector, goal posts and Inca trail were used. Modifications were made to the original design by using horn antennas for the transmitting and receiving antennas. A data acquisition system was also added to the system by using a Raspberry PI model 2. The signal processing still occurred on a computer. The authors also mention that the radar system was made lighter and possibly miniaturised.

In [11], the radar was utilised for real-time target range sensing for applications in surveillance and object detection. A car, person and class 1 drone were used as targets for measurement. Modifications were made to the original design in the following ways: i) The cantennas were replaced by commercial antennas with circular waveguides, that provided better antenna gain, ii) the RF sub-system was fabricated onto a circuit board replacing the use of the coaxial-connected microwave components, iii) the modulator, receive chain low noise amplifier and mixer circuits were also fabricated onto a circuit board and made use of an Arduino microcontroller to generate digital modulating signals that could be converted to analogue using a digital to analogue converter, These signals would be used for the tuning voltage of the oscillator. An embedded system for realtime data processing was designed, which made use of another Arduino microcontroller as an analogue to digital converter. The sampled data from the Arduino would then be sent via Wifi to a Raspberry Pi using a message queueing protocol called RabbitMQ. The

Raspberry Pi was also responsible for processing the sampled IF signal (IFFT) and then preparing the processed data for displaying the results on an external device.

In [34], the design of the authors' radar system was inspired by the MIT design. This radar was designed for ground penetration radar applications. Modifications were made to the antennas, opting to utilise planar antennas due to their superior ground penetration properties. The modulation circuit was replaced by an ARM mbed microcontroller, which was used to generate digital signals for the tuning voltage and the sync pulse required for range measurements. This also allowed a user to select from a set of modulation patterns, such as sawtooth, triangular, frequency shift keying and stepped frequency.

In [10], the radar system was used to measure the velocity and range of motor vehicles. In terms of modifications, microstrip antennas were used instead of cantennas.

In [35], the radar system was utilised for the identification of mini-unmanned aerial vehicles (UAVs), such as drones. The system combined the FMCW radar, operating with a centre frequency in between 2.4 - 2.5 GHz, together with an acoustic sensor array to form a robust detector, which covers both the high frequency band and lower audio frequency band (2 - 20 kHz).

4.5 Critical literature review

The literature review firstly recognised the effort of other authors in developing educational tools to teach RF engineering. Different commercial radar systems were also covered and their specifications were highlighted. A common feature of the commercial radars was their low power consumption and supply voltage requirements, and their ability to support multiple interfaces, such as USB, serial and Ethernet. A brief overview of the original design and purpose of the MIT coffee can radar was discussed. Lastly, literature on how other authors modified and used the radar was covered. In the literature, a recurring use for the MIT coffee can radar was for Doppler frequency and range measurement [7, 8, 9, 10, 11] and synthetic aperture radar (SAR) imaging [12, 13]. In terms of modifications performed on the radar, it was observed that other authors modified the radar by replacing its antennas [8, 9, 10, 11, 12, 13, 34] and by adding an embedded system, in the form of a microcontroller to generate the tuning voltage of the oscillator digitally [7, 11, 34].

Chapter 5

Methodology

The methodology followed to achieve the objectives set out during the project was divided into three phases. The system testing phase of the project involved developing and executing tests on the radar on a subsystem level, specifically analysing the low frequency circuits of the radar system and then performing integration testing to determine whether the radar's subsystems interfaced together correctly. Experiments were then conducted with the radar indoors and outdoors to demonstrate its capabilities in terms of measuring range and velocity. Lastly, the ISAR demonstrator prototype was designed, this involved identifying the requirements for the prototype design, construction, and the development of the radar signal processing code, experiments were then planned and conducted with the demonstrator. Throughout all the phases of the project, the research question kept in mind was: "How is the MIT S-band coffee can radar effective as an educational tool?".

Chapter 6

System testing

6.1 Purpose and scope

Before utilising the radar in the field to conduct experiments and measure radar data, it was important to test all subsystems to ensure that they were working correctly. The radar system utilised for this project was made up of three main sub-systems that interfaced with each other: i) the Radio frequency sub-system, ii) the low frequency sub-system and iii) the processing sub-system, consisting of a computer and a USB sound card. It was capable of operating in two modes: i) CW mode, to measure Doppler frequency and velocity and ii) FMCW mode, to measure range. The complete radar system is illustrated in Fig. 6.1 and its specifications are described in Table 6.2.

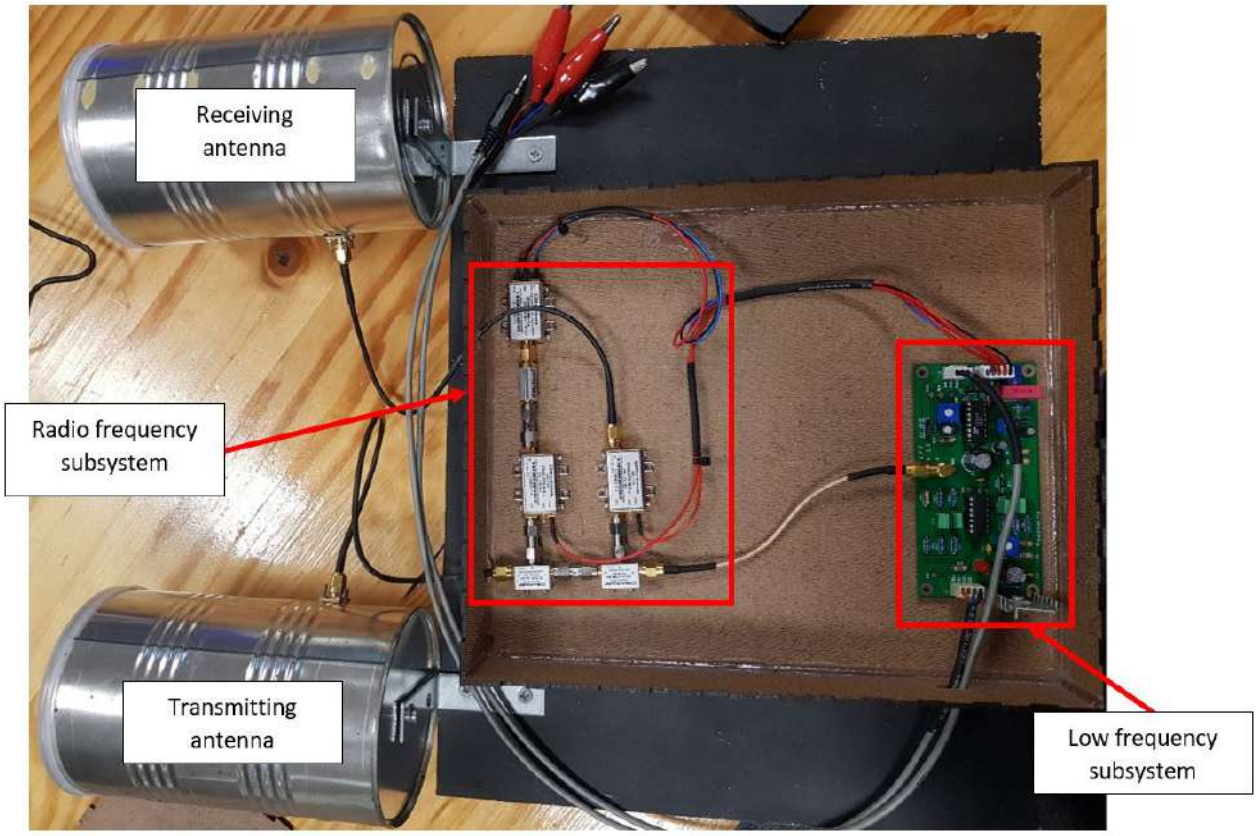

Figure 6.1: An image showing the MIT coffee can radar that was tested and utilised with its different subsystems labelled

The test procedures described in this section were performed to ensure that the radar met the initial operating specifications mentioned in Table 6.2. The tests conducted were limited to the low frequency subsystem testing and subsystem integration testing to determine whether all subsystems interfaced correctly to achieve the different operating modes of the radar: i) CW mode for Doppler measurements and ii) FMCW mode for range measurements.

6.2 Test equipment

The test procedures were conducted in UCTs White laboratory, an undergraduate electronics lab located in the department of Electrical engineering. The equipment used to conduct subsystem tests was limited to the equipment available in the lab. The equipment that was used is described in Table 6.1.

Table 6.1: The equipment used for system testing

Name	**Manufacturer**	**Model**
Digital oscilloscope	Agilent	DSO X 2002A
Digital multimeter	Agilent	34405A
Function/arbitrary waveform generator	Agilent	33220A

6.3 System specifications

6.3.1 System overview

The radar specifications are described in Table 6.2.

Table 6.2: MIT coffee can radar specifications

Design parameters	**Specifications**
Operating (center) frequency	2.445 GHz (FMCW); 2.591 GHz (CW)
FM sweep type	Triangle wave
Transmit bandwidth	180 MHz
Supply voltage	12 V
Sampling frequency	44.1 kHz
IF bandwidth	$\leq$ 22.05 kHz
Range resolution	0.8 m
Maximum range	368 m

6.3.2 Low frequency subsystem

The low frequency circuit, shown in Fig. 6.2 is made up of a modulator and low pass filter circuit. On a high level, it had two responsibilities: i) generating the required waveforms for the VCO and data processing and ii) filtering the mixer output signal, containing target frequency and phase information, that was required for further processing on a computer. Additionally, the circuit was also responsible for distributing and regulating power to different parts of the radar system.

Figure 6.2: An image showing a printed circuit board containing the low frequency subsystem of the radar system

Power supply and regulation circuit

The power supply and regulation circuit, shown in Fig. 6.3, was responsible for distributing the +12 V DC supply voltage provided by the battery pack to different locations on the circuit board. It was also responsible for regulating the + 12 V from the battery down to the + 5V DC that was required by each of the circuits in the RF subsystem. The video amplifier circuit had a voltage requirement of +12 V DC, while all of the RF circuits, except the -3 dB attenuator circuit, required + 5 V DC.

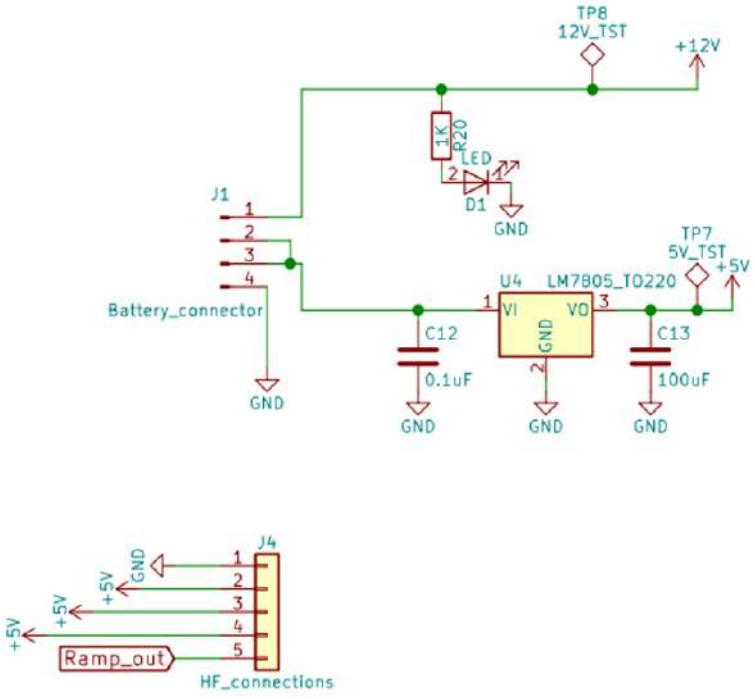

Figure 6.3: An image showing the schematic of the power supply and regulation circuit, adapted from [6]

Modulator circuit

The modulator circuit shown in Fig. 6.4 was responsible for generating two waveforms: i) the tuning voltage to control the oscillation frequency of the VCO, that generates the transmitted RF signal and ii) the synchronisation pulse (sync pulse) required for the signal processing performed on the computer when using the radar in FMCW mode. The XR2206 function generator chip was responsible for generating the required waveforms.

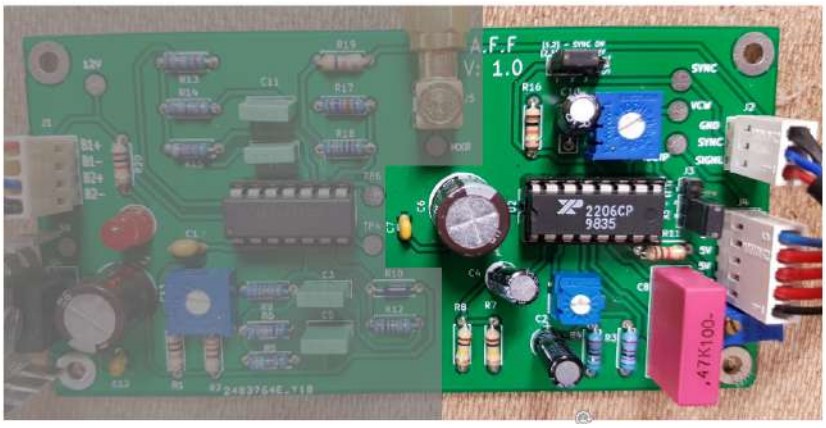

Figure 6.4: An image showing the modulator circuit found on the low frequency subsystem circuit board

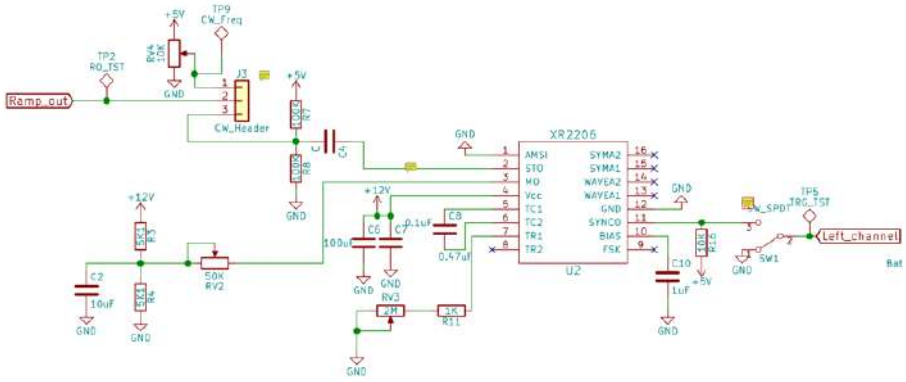

Figure 6.5: An image showing the schematic of the modulator circuit, adapted from [6]

Video amplifier circuit

The video amplifier circuit, shown in Fig. 6.6 circuit plays a vital role in filtering the IF signal output from the mixer so that it can be sampled and processed further on a computer. It is made up of two parts: i) an amplification stage and ii) a 4th order Sallen-Key low pass filter with a 15 kHz cutoff frequency, shown in Fig. 6.7. The circuit has two main responsibilities: it firstly amplifies the weak IF signal and then filters it to attenuate all unwanted high frequencies produced by the frequency mixer. The resultant signal from the circuit contains frequencies within the baseband, with frequencies up to 20 kHz, similar to the audio frequency range. This was done to ensure that the baseband signal can be sampled without any aliasing. The radar system meets the Nyquist criterion for sampling as it uses a sound card with a

sampling frequency of 44.1 kHz, more 2x the highest frequency contained in the baseband signal.

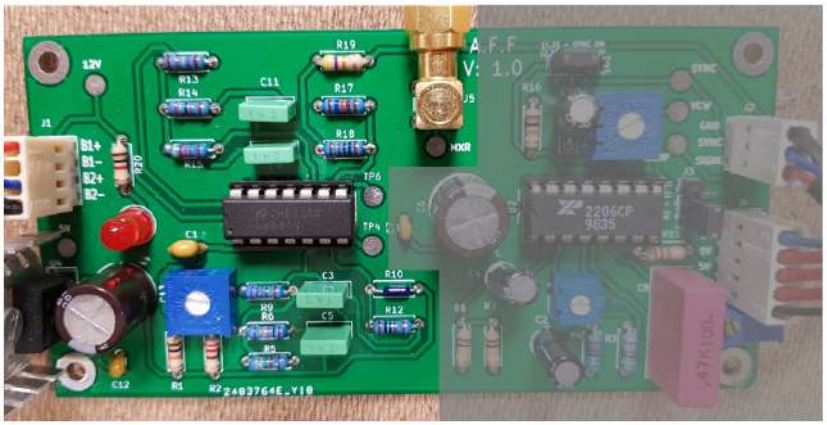

Figure 6.6: An image showing the video amplifier circuit found on the low frequency subsystem circuit board

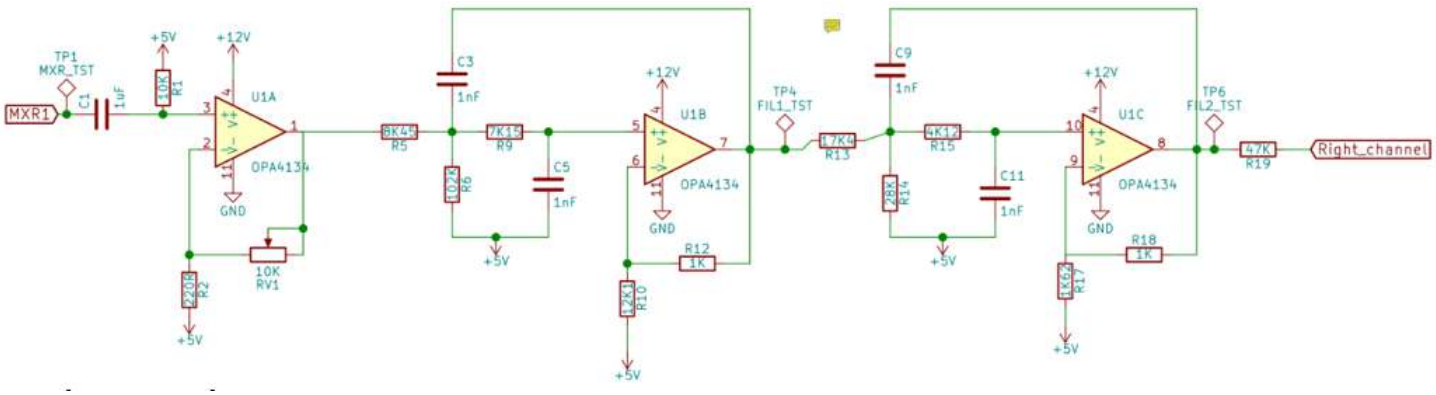

Figure 6.7: An image showing the schematic of the video amplifier circuit, adapted from [6]

6.4 Test procedures

6.4.1 Low frequency subsystem testing

Power supply and regulation circuit

This circuit provided the necessary supply voltage and was vital for the operation of the different subsystems of the radar. Therefore, it was expected that +12 V DC and +5 V DC would be measured at the supply and voltage regulator output test points of the circuit, shown in Fig. 6.8. The equipment and procedures that were followed to test the circuit are described below:

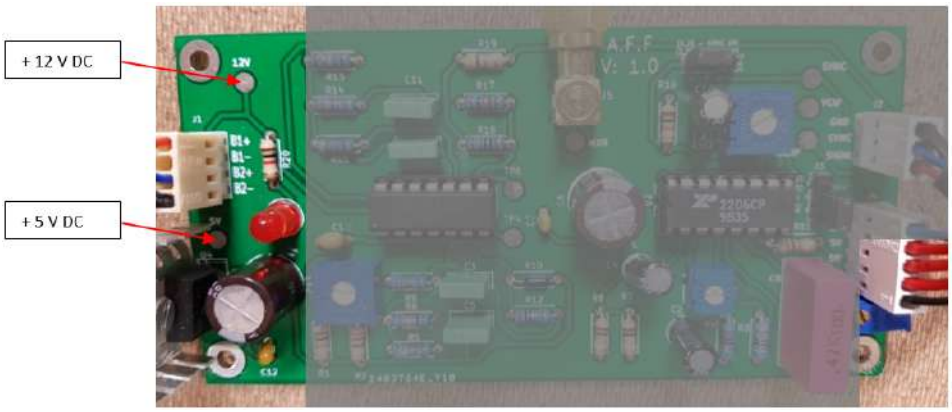

Figure 6.8: An image showing the +12 V and + 5 V DC testpoints for the power supply and regulation circuit found on the low frequency sub-system circuit board

Equipment required:

- Digital multimeter
- 12 V battery pack (together with jumper clamps)
- Appropriate red (+) and black (-) multimeter cables
- An extra pair of voltage supply cables with crocodile clips (for a stable connection to the battery clamps)

Procedure:

1. Connect the jumper cables to the 12 V battery pack. Probe the terminals of the battery pack. The multimeter should read + 12 V
2. Connect both the +B1 and +B2 terminals on the circuit to the red clamp (+) of the jumper cable and the ground (GND) terminal to the black clamp (-) of the battery pack. The extra voltage supply cables are useful to ensure a stable connection to the battery clamps. Also, the red LED on the circuit board should switch on.
3. Ground one of the multimeter cables
4. Probe on the +12 V test point. The multimeter should read +12 V.
5. Probe on the +5 V test point. The multimeter should read + 5V.

Modulator circuit

The test procedures described were performed to determine whether the modulator circuit provided the correct output waveforms to meet the operating specifications of the radar. The modulator circuit has

test points for signal probing, shown in Fig. 6.9. It also allows users to switch between the CW and FMCW mode using jumpers and has potentiometers to adjust the tuning voltage's amplitude (affecting the transmitted frequency bandwidth) and period (affecting the chirp pulse width) when using the radar system in FMCW mode. The jumpers and potentiometer are shown in Fig. 6.10.

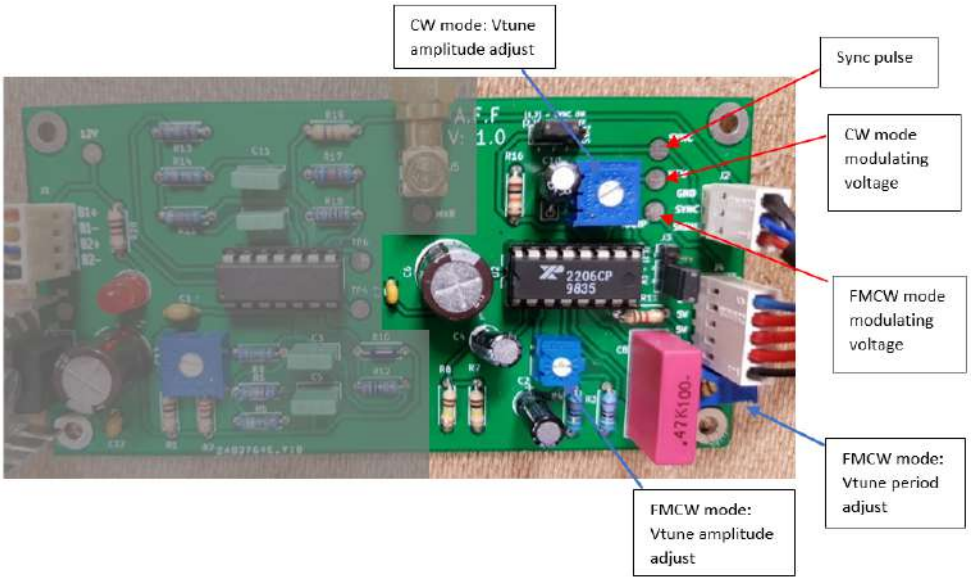

Figure 6.9: An image showing the modulator circuit testpoints for the FMCW and CW tuning voltages and potentiometers to adjust tuning voltage amplitude and period

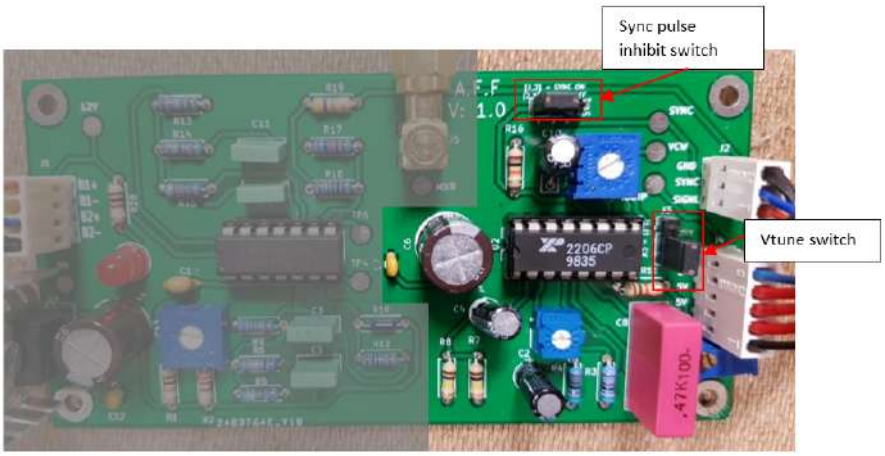

Figure 6.10: An image showing the jumpers found in the modulator circuit to disable/enable the sync pulse and switch between CW and FMCW mode

CW mode

In CW mode, a transmit centre frequency of 2.59 GHz was required to meet the required specifications for testing. Therefore, the expected tuning voltage was 5 V DC, according to the VCO's datasheet found in Appendix B.

Equipment required:

- Digital multimeter (and oscilloscope)
- Appropriate wires

Procedure:

1. Switch the radar to CW mode by using the jumpers labelled in Fig. 6.10 to switch off the sync pulse and enable the DC tuning voltage required for CW mode.
2. Switch the multimeter to DCV mode and probe on the test point labelled in Fig. 6.9.
3. Adjust the CW tuning voltage potentiometer, shown in Fig. 6.9, until the voltage reading is approximately 5 V DC.

FMCW mode

In FMCW mode, a transmit bandwidth of approximately 180 MHz was required to meet the required specifications, a triangle wave with a peak-to-peak voltage of 2.5 V was required to meet the transmit bandwidth specification. This is confirmed in Fig. 6.11 extracted from the VCO's datasheet B. By design, a +2.5 V DC offset was placed at the triangle wave output. therefore the expected transmit centre frequency would be 2.4453 GHz according to the VCO's datasheet B. Though high bandwidth is a requirement to get better range resolution, it was decided to keep the VCO operating in a linear region with respect to the tuning voltage to provide predictable behaviour.The expected specifications of the modulator circuit are described in Table 6.3.

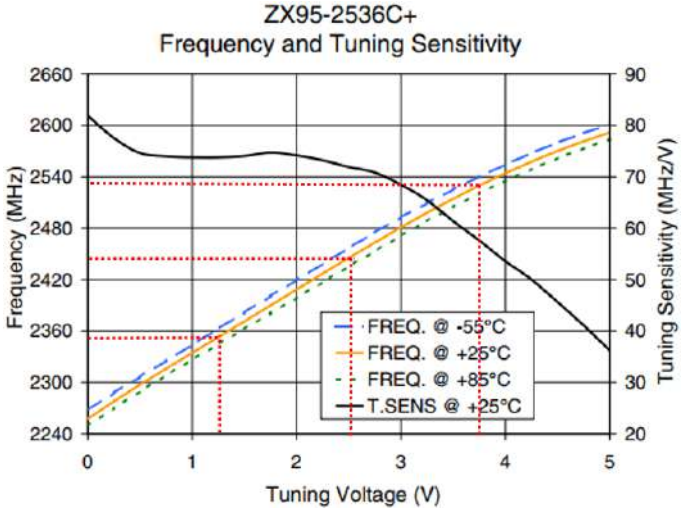

Figure 6.11: An image showing the relationship curve between the oscillation frequency of the VCO and the tuning voltage

Table 6.3: Expected specifications for modulator circuit output waveforms in FMCW mode

Parameter	**Value**
Tuning voltage waveform	Triangle wave
Tuning voltage amplitude	2.5 Vpp
Tuning voltage DC offset	+2.5 V DC
Tuning voltage period	40 ms
Sync pulse waveform	Square wave
Sync pulse period	40 ms

Equipment required:

- Oscilloscope
- Oscilloscope probes
- Small flat screwdriver

Procedure:

1. Switch the radar to FMCW mode by using the jumpers labelled in Fig. 6.10 to enable the sync pulse and the function generator's triangle wave output
2. Ground the oscilloscope probe and then probe on the i) ramp and ii) sync pulse test points, shown in Fig. 6.9.
3. Adjust the amplitude and period of the tuning voltage using the potentiometers labelled in Fig. 6.10 until the peak-to-peak amplitude reading on the oscilloscope is approximately 2.5 V and the period is 40 ms. Ensure that the sync pulse and tuning voltage have the same period.

Video amplifier circuit

The test procedures described should be performed to determine whether the video amplifier functions correctly i) amplifies and ii) filters the IF signal to meet the requirements for processing on a computer to generate range lines. The video amplifier circuit has test points for probing and a potentiometer for adjusting parameters to meet the operating specifications. The video amplifier circuit has test points for signal probing, shown in Fig. 6.12.

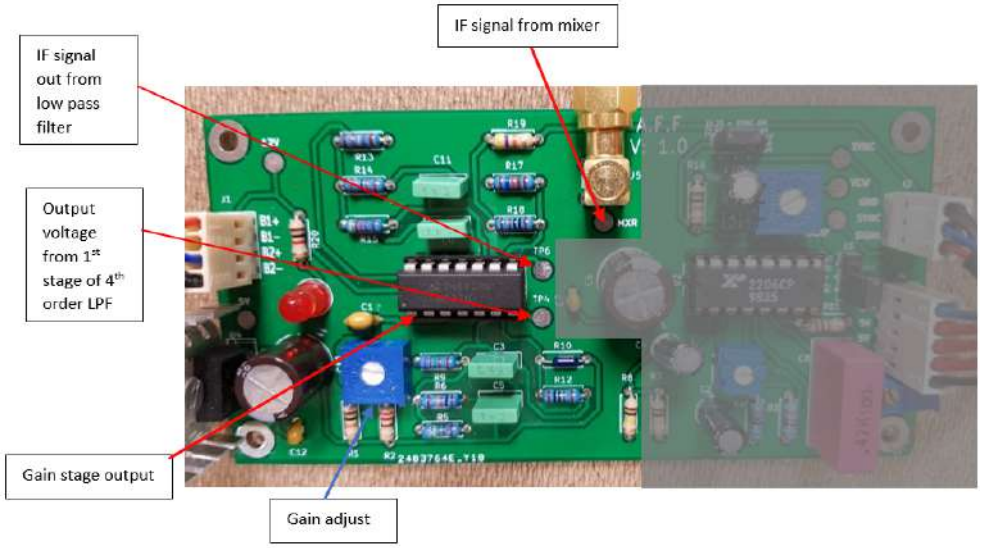

Figure 6.12: An image showing the testpoints for the video amplifier circuit found on the low frequency sub-system circuit board

Amplification stage

The amplification stage of the video amplifier is responsible for amplifying the weak IF signal received from the mixer. Therefore, it was vital to test the amplification stage to ensure that there it could adequately amplify the IF signal. The test procedures involved injecting an input signal which simulated the IF signal onto the circuit board and testing whether the amplifier worked correctly. It is also important to note that the gain of the amplifier was adjustable using the gain adjustment potentiometer labelled in 6.12 and providing a range of gains between 1 (unity gain) to 46 $\frac{V}{V}$. The expected specifications of the amplifier are described in Table 6.4.

Table 6.4: Expected specifications for the amplifier stage

Parameter	**Value**
Output gain	46 $\frac{V}{V}$
Output signal DC offset	+5 V

Equipment required:

1. Function generator
2. Oscilloscope (and scope probes)
3. SMA to crocodile clip cable (SMA cable)
4. Small flat tip screwdriver

Procedure:

1. Unscrew the SMA male to SMA male cable from the circuit board
2. Generate a 200 mV peak-to-peak sinusoidal signal with a frequency of 1.5 kHz using the function generator.
3. Measure the function generator output using the oscilloscope to ensure that the correct signal has been generated. The oscilloscope should output results as shown in Fig. 6.13

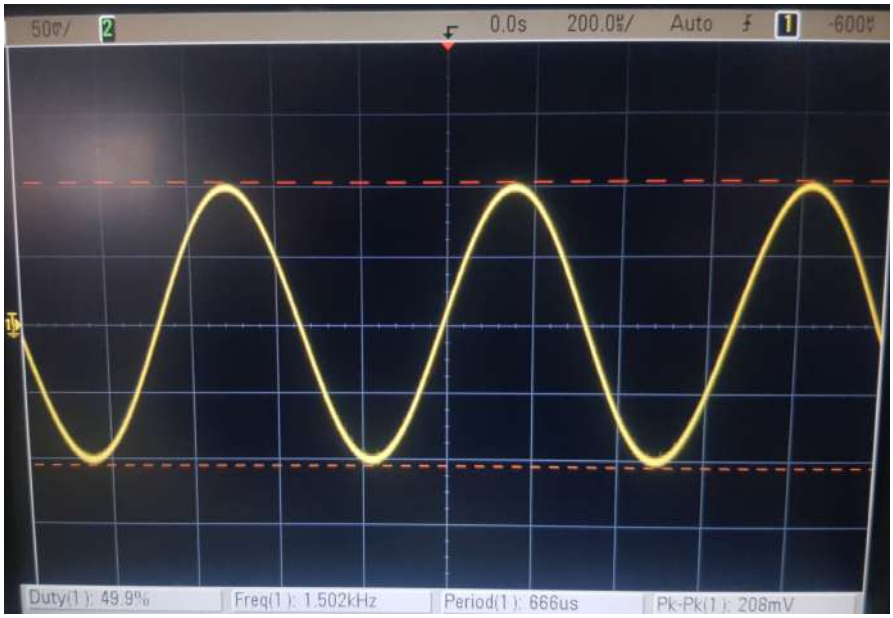

Figure 6.13: An image showing a voltage reading of a 200 mVpp sinusoidal signal with a frequency of 1.5 kHz generated by function generator

4. Screw on the SMA connector of the SMA cable to the SMA connector on the circuit board and then inject the input signal by connecting the other end of the SMA cable (crocodile clip side) to the function generator output.
5. Probe on the IF signal test point to ensure once again that the correct input signal is injected into the video amplifier. The results should be identical to Fig. 6.13
6. Adjust the gain using the gain adjust potentiometer while measuring the peak-to-peak amplitude of the output signal by probing on the IF signal test point shown in Fig. 6.12 . As the potentiometer is rotated clockwise the amplitude of the output signal should increase. Also notice that there is a +5 V DC offset on the output signal.
7. Verify that the maximum output peak-to-peak amplitude is approximately 7 V before the saturation (or clipping point) of the amplifier.

4th order low pass filter

A 4th order Sallen-Key low pass filter was responsible for filtering the IF signal received from the mixer to produce a baseband signal within the audio frequency (20 Hz - 20 kHz). This ensured that the

output signal could be sampled fast enough to be reconstructed digitally and processed on a computer. The expected specifications of the filter are described in Table 6.5

Table 6.5: Expected specifications for the 4th order Sallen-Key low pass filter

Design parameter	**Specification**
Cut-off frequency	15 kHz
Frequency roll-off	-80 dB/decade

Equipment required:

1. Function generator
2. Oscilloscope
3. SMA to crocodile clip cable (SMA cable)

Procedure:

1. Retain the connection setup in the procedure described for the amplifier testing and set the gain of the amplifier to maximum (before the saturation point).
2. Generate a 200 mV peak-to-peak sinusoidal input signal with an initial frequency of 100 Hz using the function generator.
3. Measure the peak-to-peak amplitude of the output signal using the oscilloscope as the frequency of the input signal is changed from 100 Hz to 150000 Hz, using the function generator.
4. After every frequency change, measure and record the peak-to-peak amplitude of the input and output signal and the frequency used. This can be done using a Microsoft Excel spreadsheet.
5. Once the input and output amplitudes are measured and recorded, the gain (in decibels) can be calculated using the formula Gain (in dB) $= 20 \cdot log_{10}(\frac{V_{out}}{V_{in}})$.
6. Plot the frequency response. It is expected that at a frequency of 15 kHz the gain should be 3 dB less than the passband gain and there should be a -80 dB/decade roll-off in the gain at frequencies greater than 15 kHz.

6.4.2 Radar subsystem integration testing

Once all the sub-system level tests for the low frequency circuit were performed and found to be successful the complete radar system was then tested. The complete radar system as shown in Fig. 6.1 was made of three main subsystems that interface with each other: i) the Radio Frequency system, ii) the low frequency system and the iii) Processing system, consisting of a computer and sound card; therefore, it was important to test whether the different sub-systems could work together correctly towards a complete functioning radar system that can be used to take measurements in the real world.

The test procedures described below were performed to determine whether all sub-systems interface correctly to achieve the different operating modes of the radar: i) CW mode for Doppler measurements and ii) FMCW mode for range measurements. Testing the radar in both operating modes required the same set of equipment and initial setup procedure. The Audacity digital audio software was utilised to visualise the signals sampled by the USB soundcard.

Equipment and software required:

- 12 V battery pack
- An extra pair of voltage supply cables with crocodile clips (for a stable connection to the battery clamps
- ASUS Xonar U5 USB sound card
- Computer
- Audacity audio software

Initial setup procedure:

1. Power up the radar using the +12 V battery pack similarly to the procedure in the power and regulation testing circuit.
2. Connect the USB sound card to a USB port on the computer
3. Connect the audio cable from radar to mic in port on the sound card
4. Check that it is detected by the computer by checking the sound settings. The microphone should be set to "ASUS XONAR U5".

CW mode

Procedure:

1. Switch the radar to CW mode using the appropriate jumpers (similarly to the test procedures for the modulator in CW mode)
2. Open the Audacity program and the set the microphone to ASUS XONAR U5
3. Start recording the microphone for a duration of 10-20s.
4. Wave a hand in front of radar at a distance of 20 cm

Expected results:

The left channel (top) of the signal should be inactive, indicating that the sync pulse has been inhibited correctly and the right channel (bottom) should display a fluctuating signal as a hand is wave in front of the radar.

FMCW mode

Procedure:

1. Switch the radar to FMCW mode using the appropriate jumpers (similarly to the test procedures for the modulator in FMCW mode)
2. Open the Audacity program and the set the microphone to ASUS XONAR U5
3. Start recording the microphone for a duration of 10-20s.
4. Wave a hand in front of radar at a distance of 20 cm

Expected results:

The left channel (top) of the signal should output a square wave sync pulse, indicating that the sync pulse has been activated and the right channel (bottom) should display a fluctuating signal as a hand is waved in front of the radar.

6.5 Test results

6.5.1 Low frequency subsystem testing results

Power supply and regulation circuit

The images in Fig. 6.14 and Fig. 6.15 show the measured DC voltage readings from a digital multimeter. It was expected that +12 V DC and +5 V DC would be measured at the supply voltage test point and voltage regulator output test point. In Fig. 6.14, it can be observed that a voltage of 11.9 V was measured as expected for the supply voltage line and in Fig. 6.15, a voltage of 5.09 V was measured at the voltage regulator test point as expected. It is important to note that the measured supply voltage occasionally varied and on a few occasions a voltage of 11.6 V was measured on the voltage supply test point. Therefore, it was important to keep the 12 V battery pack fully charged.

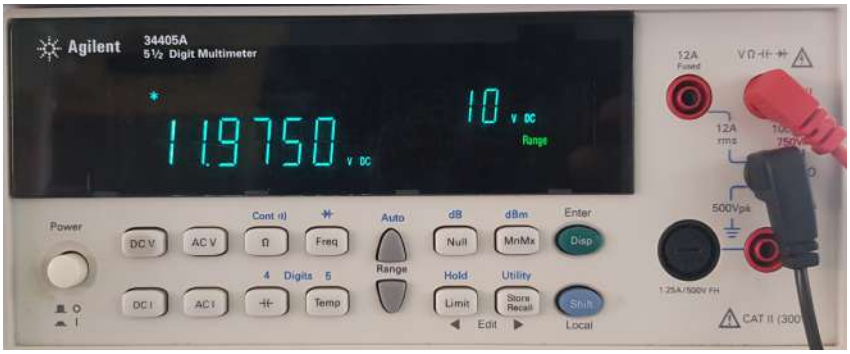

Figure 6.14: An image showing the voltage reading measured at the +12 V testpoint on the circuit board using a multimeter

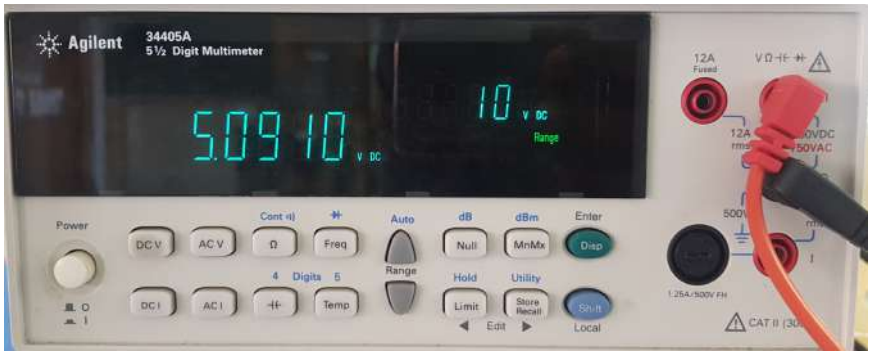

Figure 6.15: An image showing voltage reading measured at the +5 V testpoint on the circuit board using a multimeter

Modulator circuit

CW mode

In CW mode, an output tuning voltage of 5 V was required. In Fig. 6.16 the tuning voltage was measured to be 5.03 V DC as expected.

Figure 6.16: An image showing voltage reading measured at the VCW testpoint on the circuit board using a multimeter

FMCW mode

The image shown in Fig. 6.17 and Fig. 6.18 shows the measured waveforms at the ramp output and sync pulse test points. It can be observed in Fig. 6.17 that the output signal was a triangle wave as expected. The peak to peak amplitude was also measured to be 2.57 V as expected. The oscilloscope measured a DC offset of 2.32 V. This measurement was verified by measuring the DC offset using a digital multimeter set to DCV mode. This approach measured approximately 2.5 V DC as expected. In Fig. 6.18, a square waveform was measured with a period of 40 ms as required.

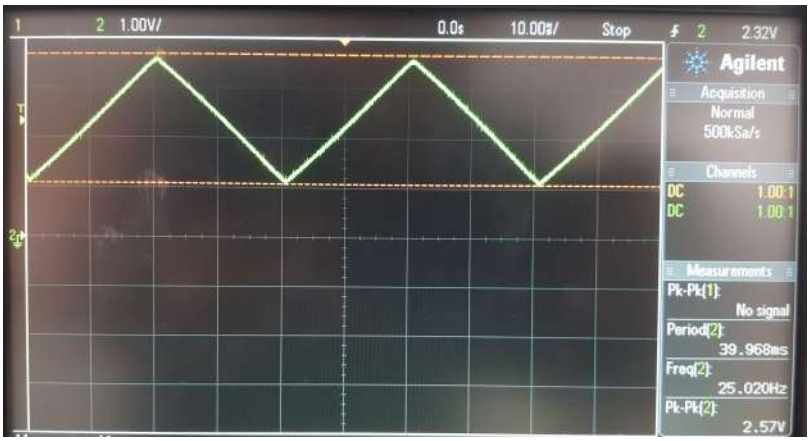

Figure 6.17: An image showing the measured 2.5 Vpp triangle wave with a period of 40 ms reading at the Ramp output testpoint on the circuit board using an oscilloscope

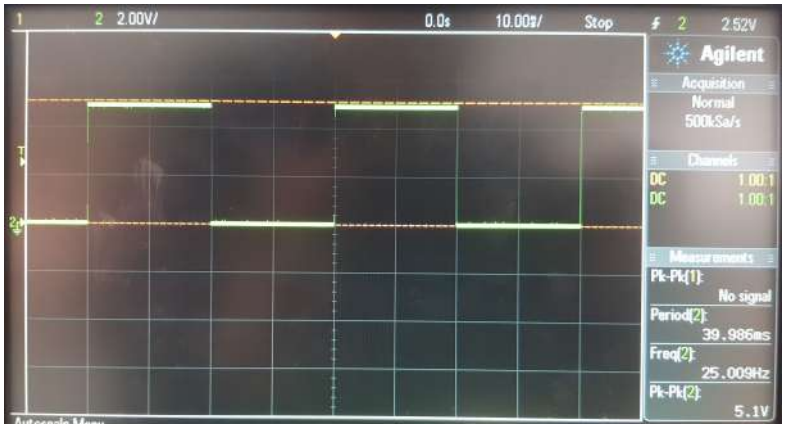

Figure 6.18: An image showing the measured 2.5 Vpp triangle wave with a period of 40 ms reading at the Ramp output testpoint on the circuit board using an oscilloscope

Video amplifier circuit

Amplification stage

The image shown in Fig. 6.19 shows the measured 200 mVpp input (green) and 7 Vpp output signal (yellow) of the amplification stage. It was expected that the maximum output gain of the amplification

stage would be 46 V/V. From Fig. 6.19, when a 200 mVpp signal was input to the amplifier, the resultant signal had a peak-to-peak amplitude of 7 Vpp. Therefore, the gain of the amplification stage was calculated to be 35 V/V. It can also be observed that the output signal has DC offset of 4.92 V, which is close to the expected 5 V.

Figure 6.19: An image showing a 200 mVpp sinusoidal wave (green) and a 7 Vpp output signal (yellow) with the same frequency of 1.5 kHz

4th order low pass filter

The image shown in Fig. 6.20 shows the measured frequency response of the low pass filter. It was expected that it would have a cutoff frequency of 15 kHz and a roll-off of -80 dB/decade. In Fig. 6.20, it was observed that the filter had a drop in gain of - 2.85 dB at 15 kHz and not the expected - 3 dB. However, this at least showed that the cutoff frequency of the filter was approximately between 15 kHz and 15.5 kHz. The roll-off of the filter was calculated to be approximately -55.1 dB/decade, indicating that the filter behaved similarly to a 3rd order low pass filter. Possible reasons for this difference in roll-off can be attributed to the tolerance of components, such as resistors and capacitors used in the filter circuit.

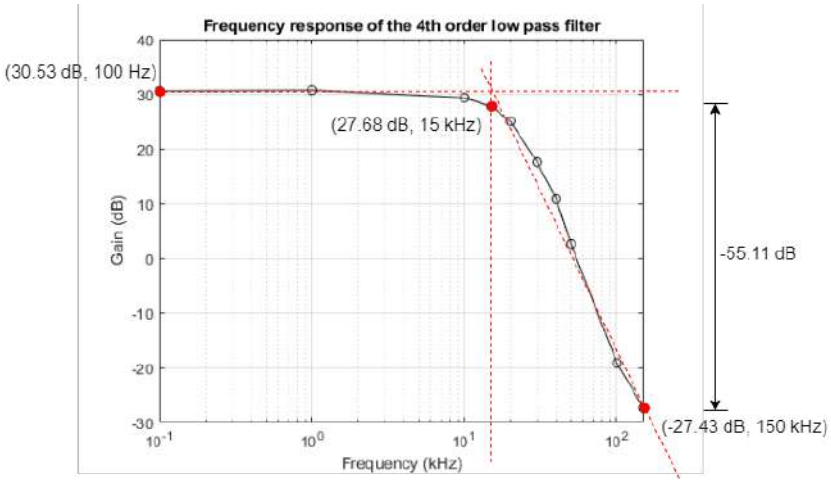

Figure 6.20: A plot showing the frequency response of the 4th order loss pass filter with a cutoff frequency of 15 kHz

6.5.2 Radar subsystem integration testing results

CW mode results

The image shown in Fig. 6.21 shows the output waveform in Audacity. In CW mode, it was expected that left channel of the signal would be disabled and that the right channel would display a fluctuating signal as proof the detection of a target, such as a hand is waved in front of the radar. In Fig. 6.21, it can be observed that the was disabled and that the baseband signal was detected on the right channel (bottom).

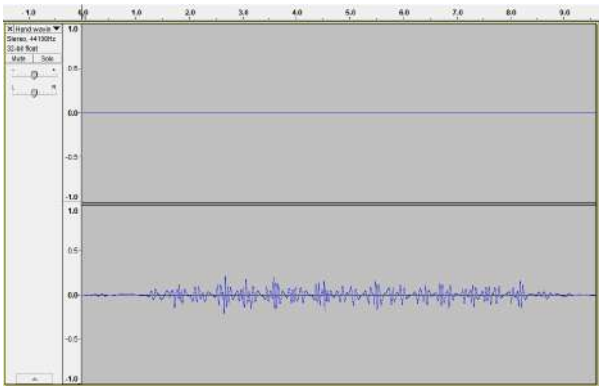

Figure 6.21: An image showing a full view of the sampled output signal from the low frequency subsystem in CW mode using the Audacity digital audio software. The left channel (top) shows a disabled sync pulse and the right channel (bottom) shows the baseband signal received

FMCW mode results

The image shown in Fig. 6.22 shows the output waveform in Audacity. In FMCW mode, it was expected that left channel of the signal would output a square wave sync pulse, indicating that the sync pulse has been activated and that the right channel would display a fluctuating signal as proof the detection of a target, such as a hand is waved in front of the radar. In Fig. 6.22, it can be observed that the synchronisation square wave was detected on the left channel (top) and that the baseband signal was detected (bottom). The full image of Fig. 6.22 showing the fluctuations of the baseband signal can be found in Appendix C.

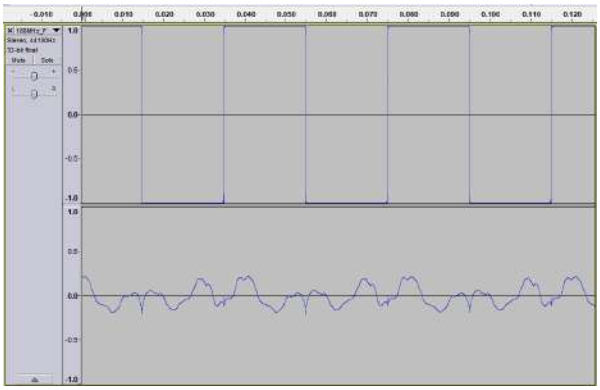

Figure 6.22: An image showing the sampled output signal from the low frequency subsystem in FMCW mode using the Audacity digital audio software. The left channel (top) shows an enabled sync pulse and the right channel (bottom) shows the baseband signal received

6.6 Conclusion

The aim of this section was to develop and execute sub-system tests that could be performed before making use of the radar system to measure radar data. These tests were developed and executed successfully. Most of the tests were passed, however a few deviations from the expected results were also observed, such as in the frequency roll-off of the 4th order low pass filter and the maximum gain of the amplifier stage found in the video amplifier circuit. It was also observed that the supply voltage also varied depending on whether the 12 v battery pack was fully charged or not. It was concluded that the radar system was in a good working condition and could be used for further experimentation.

Chapter 7

Indoor and outdoor experiments

This chapter covers the procedures and results from experiments performed to demonstrate the MIT coffee can radar's range and Doppler frequency measuring capabilities. Indoor and outdoor experiments were developed and executed to experiment with the radar in different settings.

7.1 Range experiments

7.1.1 Measuring the range of multiple human targets in the White lab

This experiment involved utilising the radar in FMCW mode to measure the range of multiple targets. The experiment setup used to perform the experiment is shown in Fig. 7.1.

Experiment setup

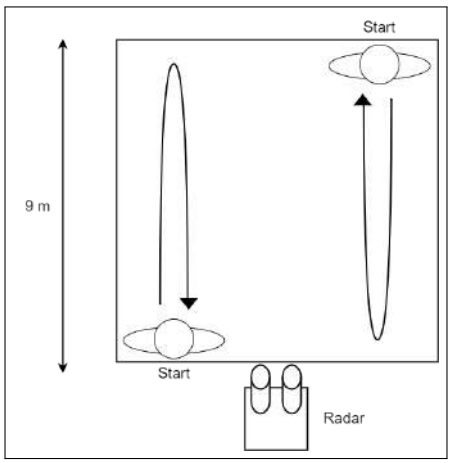

Figure 7.1: A diagram showing the setup used to measure the range of two human targets over time

Results

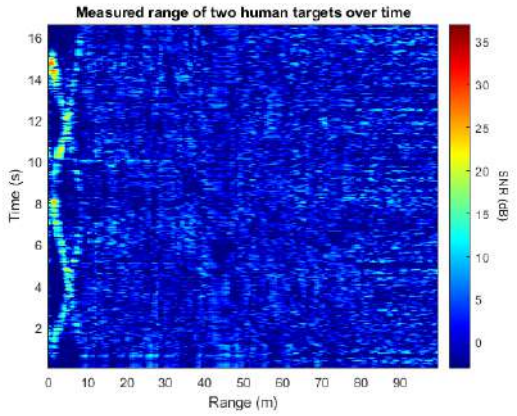

Figure 7.2: A plot showing the range of two human targets over time while moving in opposite directions over a distance of 9m, in front of the radar system (PRI = 40 ms)

The measured range over time of the human target is shown in Fig. 7.2. It can be observed in Fig. 7.2 that the radar was able to track the two human targets and it estimated the range to be between 9-10 m.

7.1.2 Estimating the dimensions of the White lab

Experiment setup

To estimate the dimensions of the White lab, the radar system and target were set up as shown in Fig. 7.4. The radar system was then set up using the specifications listed in Table 7.2. This experiment involved having a human target walk away from radar and then back to it.

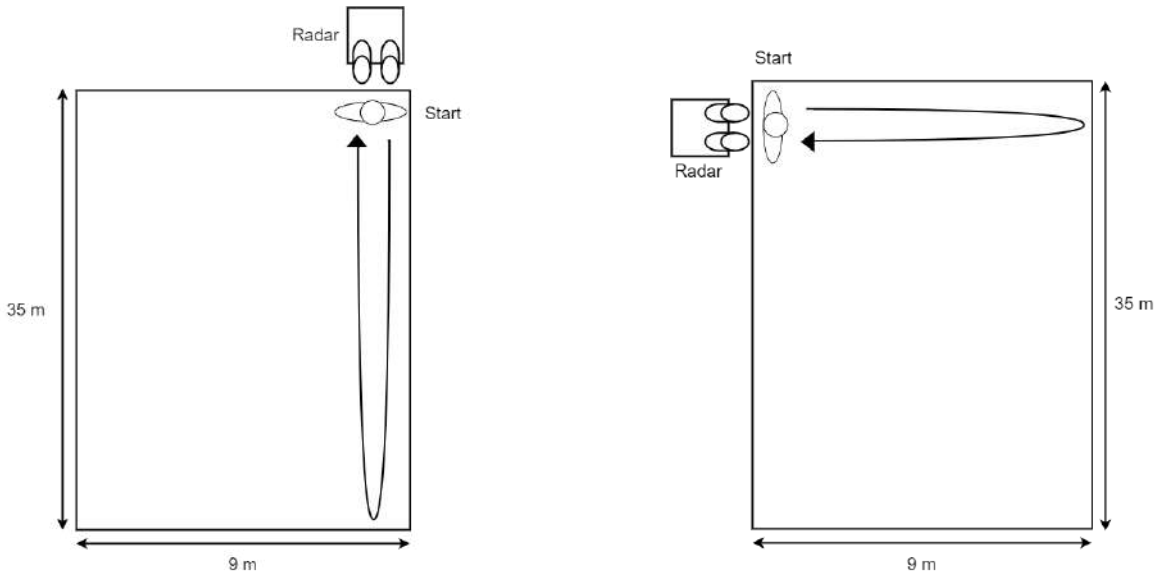

(a) Length measurement setup

(b) Width measurement setup

Figure 7.3: A diagram showing the setup used to estimate the dimensions of the White lab

Table 7.1: Radar system specifications for Doppler experiments

Parameter	**Specification**
Center frequency	2.445 GHz
RF Bandwidth	177 MHz
PRI	40 ms

Results

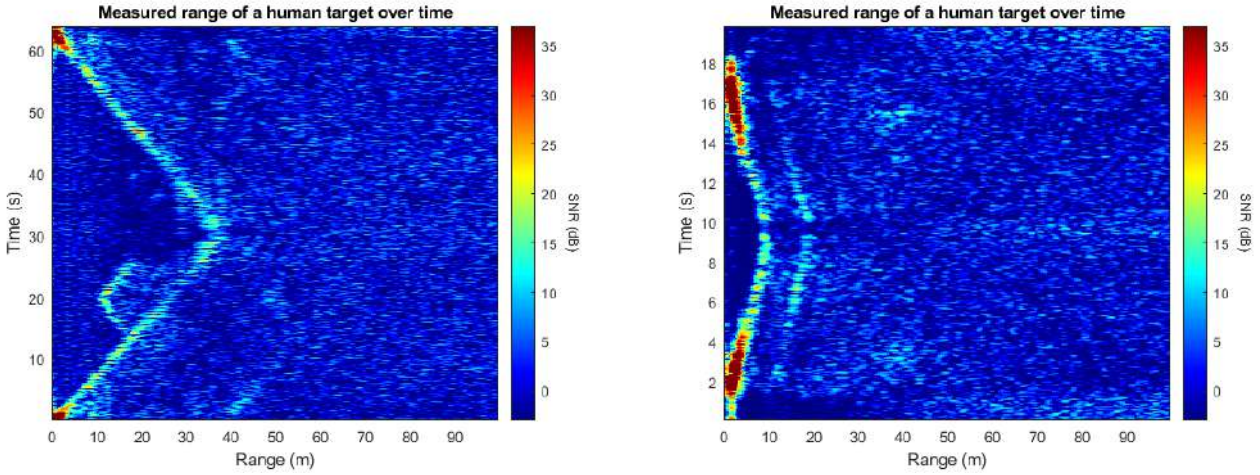

(a) Length measurement

(b) Width measurement

Figure 7.4: Plots showing the measured range of a human target over time while walking a) the length and b) the width of the White lab

The measured range over time of the human target is shown in Fig. **??**. It can be observed in Fig. 7.4a that the radar was able to estimate a distance of 35-40 m and it can be observed in Fig. 7.4b, that the radar was able to measure a width of 9-10 m. In both, Fig. 7.4a and Fig. 7.4b it can be observed that other targets were also identified during the test. In Fig. 7.4a, from 15 to 25 s another target was detected at a range of 10-20 m while measuring and in Fig. 7.4b, another target was detected at a range of 10-20 m between 6-14 s. These targets were other human targets present in the lab or nearby buildings.

7.1.3 Determining the maximum range of the radar for human targets

Experiment setup

To determine the maximum range of the radar for human targets, the radar system and target were set up as shown in Fig. 7.5. The radar system was then set up using the specifications listed in Table 7.2. This experiment involved having a human target walk away from radar and then back to it. This was conducted on the UCT rugby field and involved the target walking the 100 m length of the rugby field.

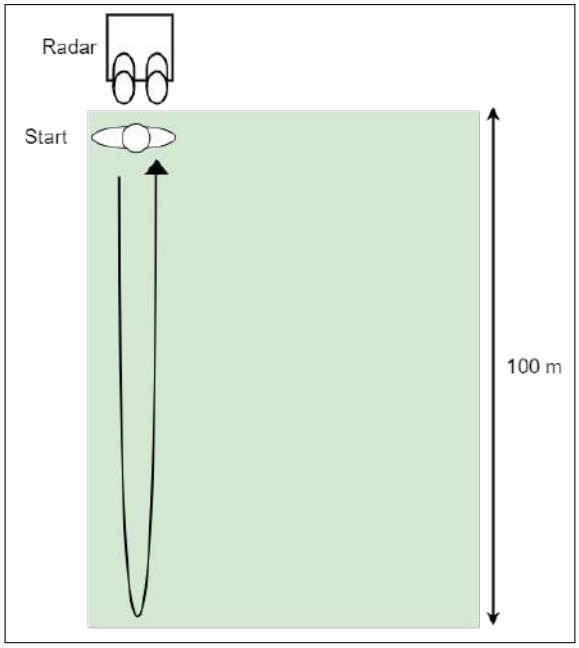

Figure 7.5: A diagram showing the setup used to estimate the maximum range of the radar for human targets

Table 7.2: Radar system specifications for Doppler experiments

Parameter	**Specification**
Center frequency	2.445 GHz
RF Bandwidth	177 MHz
PRI	40 ms

Results

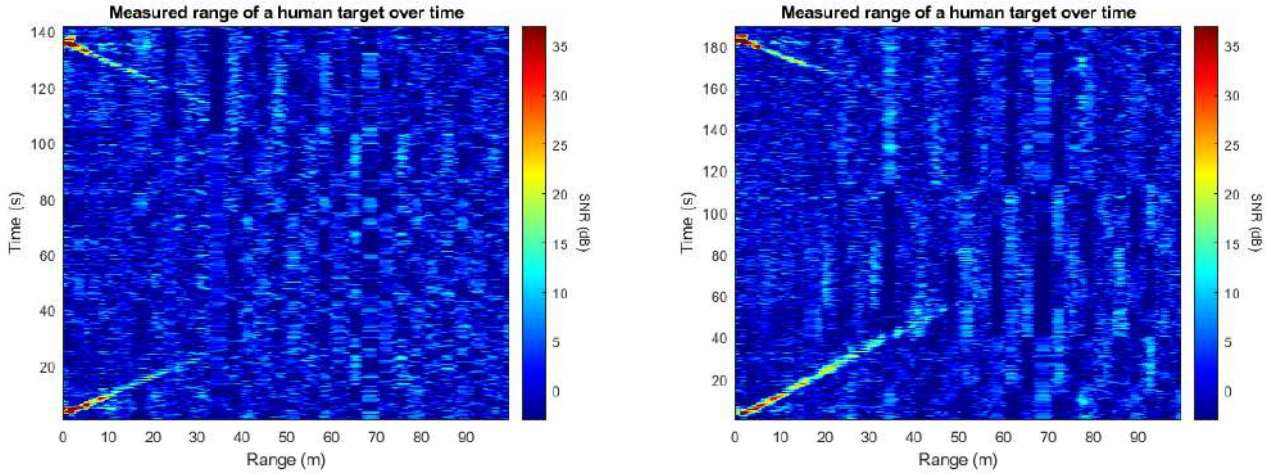

(a) Test 1

(b) Test 2

Figure 7.6: A plot showing the range of a human target over time while walking towards the 100 m rugby line and back towards the radar system (PRI = 40 ms)

The measured range over time of the human target is shown in Fig. 7.6. In Fig. 7.6a, it can be observed that the radar was able to track the human target for approximately 20 s, after 20 s as the target moved further from the radar, the signal to noise ratio in the reflected signal decreased, approaching 0 dB. It can be observed in Fig. 7.6a and Fig. 7.6b that the estimated maximum range of the target appears to be between 30 - 60 m. In other experiments conducted, in the field, with an the PRI was increased, the maximum range when tracking human targets appeared to be between 30 - 50 m. Those results can be found in Fig. D.2-D.5 in Appendix D.

7.2 Doppler experiments

7.2.1 Measuring the speed of moving human targets

Experiment setup

To measure the speed of moving human targets in the lab, the radar system and target were set up as shown in Fig. 7.7. The radar system was then set up using the specifications listed in Table 7.3. This experiment involved having a human target walk, jog and then sprint towards the radar.

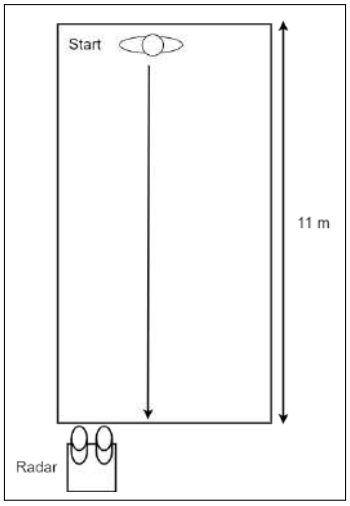

Figure 7.7: A diagram showing the setup used to measure the speed of human targets, in the White lab

Table 7.3: Radar system specifications for Doppler experiments

Parameter	**Specification**
Center frequency	2.591 GHz
PRF	50 Hz

Results

Human target slowly walking towards radar

The plot shown in Fig. 7.8 shows the measured speed over time of a human target walking slowly towards the radar system. The radar transmitted at a PRF of 50 Hz and was located at a distance of 11 m away from the starting position of the target. In Fig. 7.8, it can be observed that the radar measured maximum speed of 0.5 to 1 m/s.

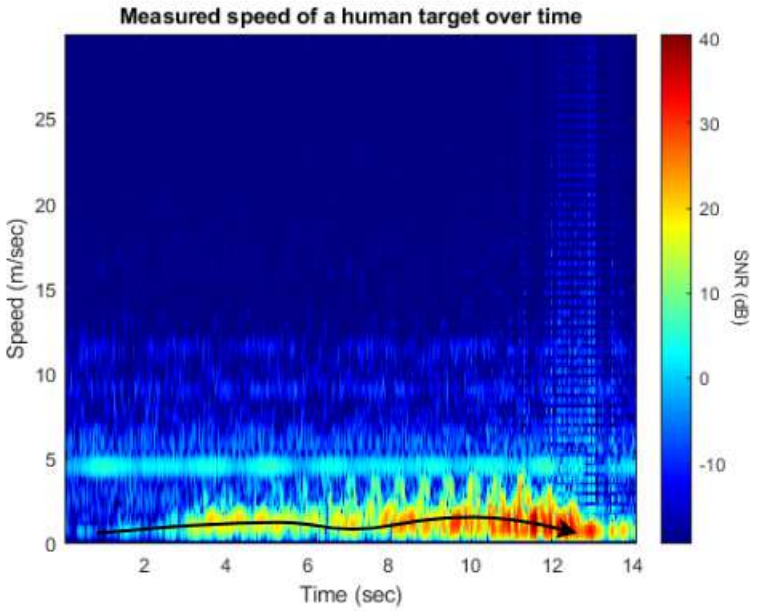

Figure 7.8: A plot showing the measured speed over time of a human target walking slowly towards the radar (PRF = 50 Hz)

Human target jogging towards radar

The plot shown in Fig. 7.9 shows the measured speed over time of a human target jogging towards the radar system. The radar transmitted at a PRF of 50 Hz and was located at a distance of 11 m away from the starting position of the target. In Fig. 7.9, it can be observed that the radar measured a maximum speed of 2 to 2.5 m/s.

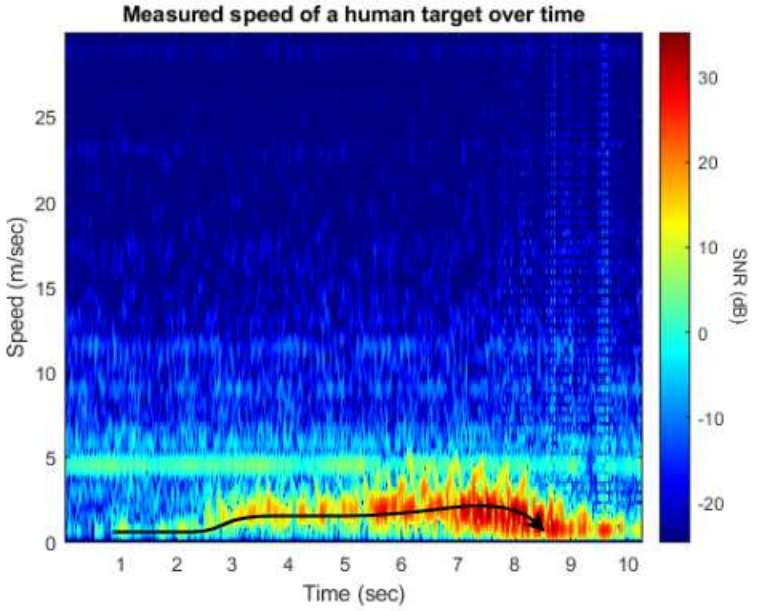

Figure 7.9: A plot showing the the measured speed over time of a human target walking slowly towards the radar (PRF = 50 Hz)

Human target sprinting towards radar

The plot shown in Fig. 7.10 shows the measured speed over time of a human target sprinting towards the radar system. The radar transmitted at a PRF of 50 Hz and was located at a distance of 11 m away from the starting position of the target. In Fig. 7.10, it can be observed that the radar measured a maximum speed of 4 to 5 m/s.

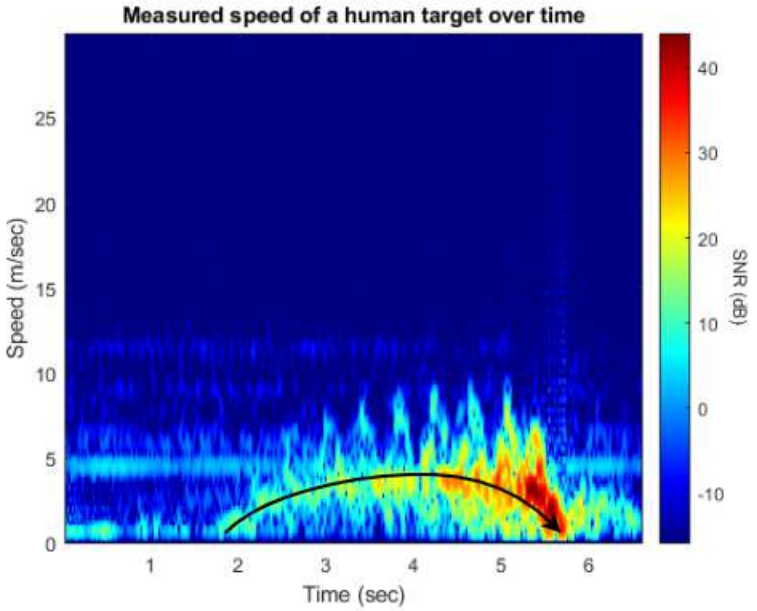

Figure 7.10: A plot showing the the measured speed over time of a human target walking slowly towards the radar (PRF = 50 Hz)

Chapter 8

ISAR imaging prototype design

This chapter describes the design process of an ISAR imaging prototype using the MIT radar. The goal of this phase of the project was to determine if it would be feasible to develop an ISAR demonstrator using the MIT radar in FMCW mode.

8.1 Requirements and design choices

From the ISAR theory, the imaging process relies on the motion of the target being imaged. Due to the fact that this design would be a proof of concept, it was decided that ISAR imaging would be performed using a rotating turntable experiment, where the target would rotate on a platform. This experiment limits the amount of non-cooperative target motion [2]. This means that the target moves in a controlled manner and the expected results for the image would be known beforehand. This section discusses the requirements related to the ISAR demonstrator system.

8.1.1 Rotational motion

The rotational motion of the target needed to be achieved through some mechanism. This meant that a rotating platform was needed to achieve this, within the project budget and time constraints. There were two possible design options to achieve this requirement: constructing a complete platform by possibly utilising servo motors attached to a base platform and controlling them using a microcontroller, such as an Arduino or buying an already made rotating platform and assessing if the platform's rotation rate was suitable for ISAR imaging. Due to the time constraints of the project, the 2nd option was selected and a turntable was purchased (shown in Fig. 8.1). This was seen as the better option given the budget and time constraints of the project. This option also required less engineering effort to get multiple components working together. However, this option also had its disadvantages because the turntable was limited to two speed settings: 3-4 revolutions per minute (RPM) and 6-8 RPM and had its base platform had a small circular diameter of 20 cm.

Figure 8.1: An image showing the initially acquired turntable for the ISAR imaging rotating platform

8.1.2 Target type

A target with good reflective properties would need to be utilised to ensure a high signal-to-noise ratio and to prevent the need to perform data collection multiple times. The target size and weight would also be a consideration as it would need to be placed on the turntable. Corner reflectors were selected as ideal targets for imaging because they are known to provide a strong signal return and are often used for SAR imaging calibration. It was decided that the corner reflectors would be constructed and that the goal would be to determine whether the radar system could produce an image of three adjacent corner reflectors in the target scene.

8.1.3 Signal processing

Once the signal data would be collected, processing would need to be performed on the data in software to generate range-Doppler maps and confirm whether ISAR imaging would be feasible with the radar. It was decided that the MATLAB environment would be utilised due to its extensive signal processing functionality and ease of use.

8.2 Design calculations

Once the turntable was acquired, calculations were performed to determine the required configuration settings for the radar system to perform imaging without the targets aliasing. Both the fast and slow settings of the turntable were considered for the experiment. The centre frequency was set to be 2.4 GHz and the transmit bandwidth, B, of the radar was kept at 180 MHz because a high resolution is required for ISAR imaging. Therefore, the expected range resolution of the radar was 0.83 m. It was also decided to place the corner reflectors at a radius, R, of 0.5 m from the centre of rotation.

As mentioned in Chapter 2, the PRF of the radar waveform transmitted determines whether the target's Doppler frequency is measured unambiguously or not. The calculations below summarise the process of determining the correct PRF for the radar waveform for the experimental setup shown in Fig. 8.2.

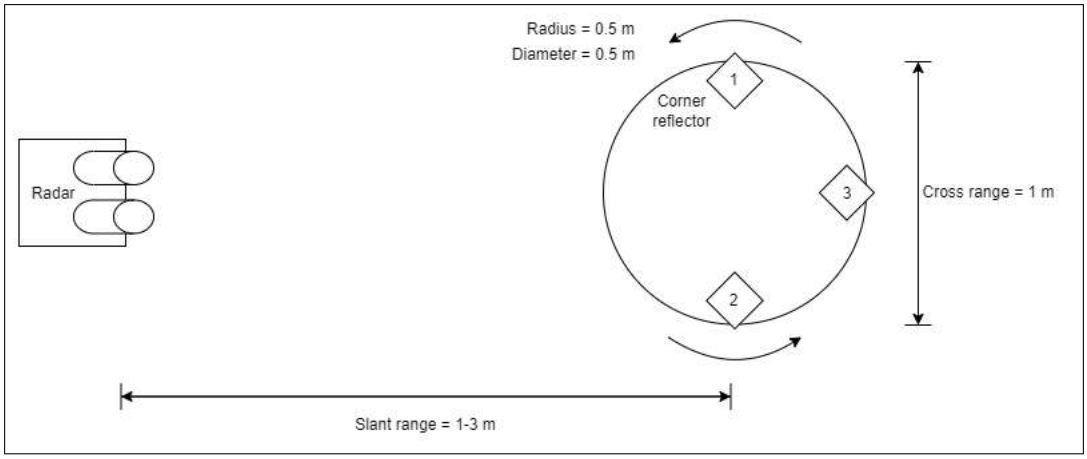

Figure 8.2: ISAR imaging experiment setup for a short observation window of rotating corner reflectors set a 0.5 m from the center of rotation and slant range of 1-3 m

The calculations performed depended on the turntable's speed setting and angular velocity, Ω, to determine the i) maximum target radial velocity , $v_{r(max)}$, ii) maximum target Doppler frequency, $f_{d(max)}$ and iii) PRF required. Equations 8.1 - 8.3 were used for these calculations.

$$v_{r(max)} = \Omega \cdot R \tag{8.1}$$

$$f_{d(max)} = \frac{2v_{r(max)}}{\lambda_t} \tag{8.2}$$

$$PRF = 2 \cdot f_{d(max)} \tag{8.3}$$

8.2.1 Slow turntable setting

The average speed of the turntable was considered as 3.5 RPM, which resulted in an angular velocity, $\Omega = 0.367$ rad/s. The maximum target velocity was calculated to be $\pm$ 0.183 m/s. This meant that the corner reflectors labelled 1 and 2, in Fig. 8.2 would each have a detectable radial velocity with opposite signs, due to their opposing directions of motion. However, the third corner reflector would have a radial velocity equal to zero as it would appear stationary to the radar. The maximum Doppler frequency was calculated to be approximately 3 Hz. Therefore, the required PRF would need to be at least 6 Hz or greater to measure unambiguous Doppler frequency.

8.2.2 Fast turntable setting

Similar calculations were performed for the fast setting of the turntable, using an average speed of 7 RPM ($\Omega = 0.733$ rad/s). $v_{r(max)}$ was calculated to be $\pm$ 0.367 m/s, therefore $f_{d(max)}$ was equal to 6.09

Hz. The required PRF would need to be at least 12.18 Hz or greater to measure unambiguous Doppler frequency. The radar specifications can be summarised in Table 8.3.

Table 8.1: Radar system specifications for ISAR imaging

Turntable setting	**Average angular velocity, Ω**	**PRF**
Slow	0.367 rad/s	At least 6 Hz
Fast	0.733 rad/s	At least 12 Hz

8.3 Platform and corner reflector construction

8.3.1 Platform

The base of the turntable bought was limited in its diameter (20 cm). Therefore, additional material was acquired to extend its size. The size and weight of the material were also considered as this would affect the load on the turntable's motors and could vary the speed of the rotating platform. A 640 x 460 cm sheet of hardboard was acquired and attached to the original base of the turntable. This provided a wider and stable base for any additional material. Strips of 60 cm x 23 cm corrugated cardboard were then attached on top of the hardboard base, together with prestik and cellotape, to achieve the necessary separation between the corner reflector targets. Once the modified base platform was placed on the turntable it was found that the actual angular velocities, Ω, for the two turntable speed settings were 0.380 rad/s for the slow setting and 0.676 rad/s for the fast setting. This change was due to the added weight of the modified platform. The material used and modified turntable are shown in Fig. 8.3 and Fig. 8.4.

Table 8.2: Actual specifications of rotating platform for ISAR imaging

Turntable setting	**Actual angular velocity, Ω**
Slow	0.380 rad/s
Fast	0.676 rad/s

Figure 8.3: An image showing the materials that were utilised to construct the base of the rotating platform

Figure 8.4: An image showing the final rotating platform utilised for the ISAR imaging experiments

8.3.2 Corner reflectors

For the targets, three 12 cm x 12 cm x 12 cm corner reflectors were also constructed. This involved making use of corrugated cardboard, aluminium foil and craft glue. The corner reflectors are shown in Fig. 8.5 and 8.6.

Figure 8.5: An image showing the corner reflector construction setup showing three 12 x 12 x 12 cm corner reflectors made out of corrugated cardboard and aluminium foil

Figure 8.6: An image showing the final corner reflectors used for the ISAR imaging experiments

8.4 Digital signal processing software design

Once the platform was constructed, the algorithm to generate the range-Doppler maps of the corner reflectors using the radar system in FMCW mode was planned and then implemented in MATLAB code. On a high level, the imaging process can be divided into three main steps shown in Fig. 8.7.

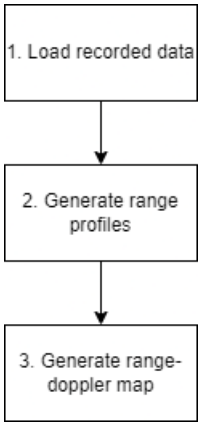

Figure 8.7: A diagram showing an overview of ISAR image reconstruction process

Once the reflected signals are received at the radar system, they are mixed with the transmitted RF signal, also known as the local oscillator (LO), to generate an IF signal. This IF signal is then amplified and passed through a low pass filter to retain all the frequencies within the 20-20 kHz (audio frequency range), producing a baseband signal containing frequency and phase information related to the target scene. The output audio signal received at the USB sound card via the 3.5 mm audio jack contains: i) the synchronisation square wave pulse generated by the modulator circuit and ii) the baseband signal from the mixer, in its left and right channel, respectively. The recording process at the USB soundcard involves sampling the audio signal at a sampling frequency of 44.1 kHz and saving the recording in a .wav audio file. These recorded files are then loaded into MATLAB for further processing.

8.4.1 Range profiling

Before the range profiles of the targets are generated some pre-processing was performed on the audio signal. Once the left and right channels of the signal were extracted, the indices of the rising edges of the synchronisation pulse (sync pulse) were found and stored by parsing the sync pulse. This information located the starting position of each pulse, allowing the estimation of the chirp pulse length, the number of pulses transmitted within the observation window and the number of samples to store from the baseband signal. This also ensured that processing only occurred on the signal data contained within the rising edge of the triangular wave.

Once the number of pulses transmitted, N, and the number of samples to consider within the chirp pulse width, M, were determined, an empty NXM matrix, with N rows and M columns, was created to store this data. For each pulse index, N, the time domain audio signal was time-aligned with the trigger event of the sync pulses, ensuring that correct signal samples were collected. A Hann window was then applied to the time domain audio signal to decrease the side lobes in the frequency spectrum of the signal. The frequency spectrum of the audio signal was then generated by applying the Fast Fourier Transform (FFT) algorithm and then the appropriate time delay was applied in the frequency domain by multiplying the spectrum with a complex exponential signal. Lastly, the range profiles associated with each pulse were produced by applying the Inverse FFT and were then stored at each row index of the NxM matrix. The

rows in the matrix correspond to the range profiles and the columns correspond to the range bins.

The range profiles acquired in the NxM matrix also contained returns from stationary targets, therefore the Moving Target Indicator (MTI) algorithm was applied to minimise the stationary targets in order to observe the range migration of the moving targets.

8.4.2 Range-Doppler mapping

Once the range profiles were acquired, profiles over a short observation window were extracted. This depended on the number of pulses to consider and the turntable speed setting set by the user. A short observation window was chosen to minimise the range migration of the targets and to avoid having to apply range alignment algorithms on the range profiles. A Hamming window was applied over each column of the extracted range profiles, to reduce the side-lobes of the signal data in the frequency domain. Lastly, the range-Doppler map representing an image of the target scene was then reconstructed by applying the FFT algorithm over each range bin for all pulses considered in the short observation window. Multiple ISAR images are produced by considering multiple short observation window frames that overlap each other by 50% over a long audio recording.

A link to the code written can be found in Appendix A.

8.5 Experimental setup

To collect radar data, the rotating platform and radar system were set up as shown in Fig. 8.8. The radar system was then set up using the specifications listed in Table 8.3.

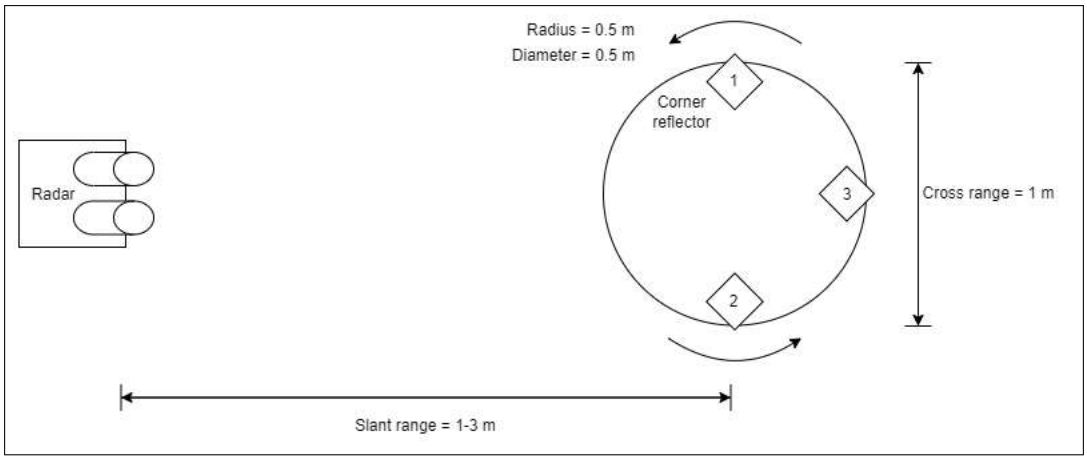

Figure 8.8: A diagram showing a top down view of the ISAR imaging experiment setup for a short observation window with rotating 3 corner reflectors set a radius of 0.5 m from the center of rotation and slant range of 1-3 m

Table 8.3: Radar system specifications for ISAR imaging experiments

Parameter	**Specification**
Center frequency	2.445 GHz
RF Bandwidth	177 MHz
PRF	20 Hz
PRI	0.05 s
CPI	0.80327 s
Range resolution	0.83 m
Doppler resolution	1.25 Hz
Cross-range resolution	0.194 m (slow); 0.113 m (fast)
Ramp modulation	Triangle wave

The experiment procedure involved firstly configuring the radar to the specifications shown in Table 8.3 and then considered imaging the corner reflectors in four cases listed below:

- Case 1 involved setting the radar at a slant range of 1 m and placing one corner reflector on the platform, 0.5 m away from the centre of rotation.
- Case 2 involved setting the radar at a slant range of 2.5 m and placing one corner reflector on the platform, 0.5 m away from the centre of rotation.
- Case 3 involved setting the radar at a slant range of 1 m and placing two corner reflectors on the platform, as shown in Fig. 8.2, 0.5 m away from the centre of rotation.
- Case 4 involved setting the radar at a slant range of 2.5 m and placing two corner reflectors on the platform, 0.5 m away from the centre of rotation.

The turntable was then set to its slow or fast setting and allowed to rotate. The Audacity digital audio software was utilised to capture 1 minute long recordings for different turntable speed settings and slant ranges from the radar system. At least two trials of radar measurements were taken to ensure consistency in the measurements. The results presented in and discussed in section 8.6 were generated using slow speed setting. The resultant additional images of corner reflectors rotating at a fast speed can be found in Appendix E

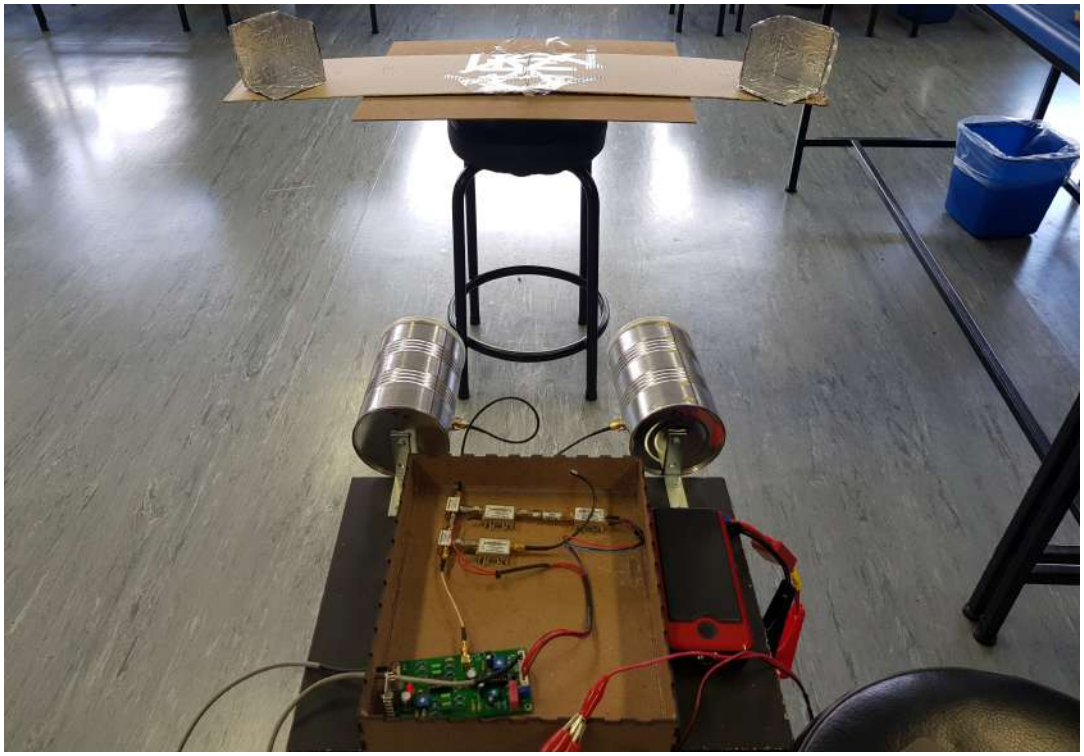

Figure 8.9: An image showing the actual ISAR imaging setup in the lab, with the radar system 1 m away from the rotating platform

8.6 Results and Discussion

8.6.1 Case 1: One corner reflector located at a slant range of 1 m rotating at a slow speed

The resultant images shown in Fig. 8.10 were generated for one corner reflector target rotating at an angular velocity, Ω of 0.380 rad/s, at a radius of 0.5 m of the rotating platform's centre of rotation. The radar was placed at a slant range of 1m away from the rotating platform. The radar system transmitted at a PRF of 20 Hz and an observation window of 0.8 s was considered, equivalent to 16 pulses, to limit the amount of range bin migration. The first observation from Fig. 8.10 is that the radar system was able to detect one corner reflector. The expected Doppler frequency was ± 3.2 Hz, however, from the image, the radar estimated a Doppler frequency between 1.245 Hz and 3.735 Hz at the locations with the highest signal intensities. The expected cross-range was 0.5 m, however from the image, the radar estimated a cross-range between 0.192 m and 0.578 m. The expected slant range was 1 m, however, the slant range of the corner reflector was observed to be between 1-2 m at the locations on the Range-Doppler map with the highest signal intensities.

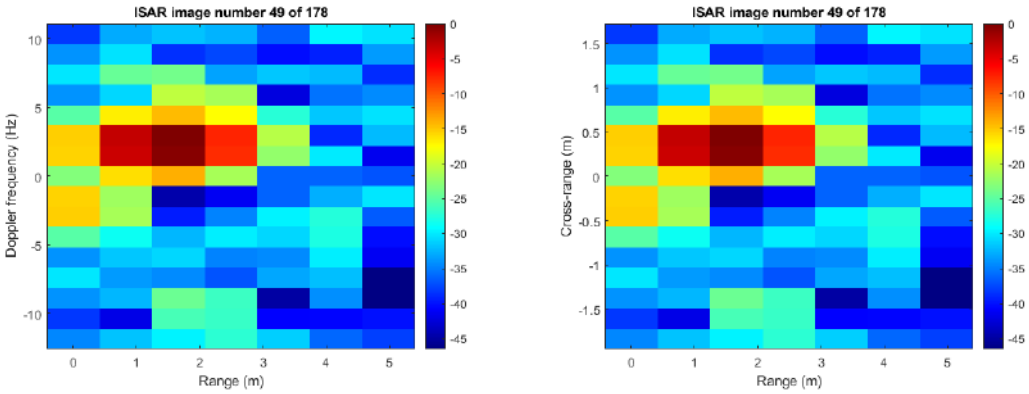

(a) Doppler frequency vs Range map (b) Cross-range vs Range map

Figure 8.10: Resultant ISAR images for one corner reflector located at a slant range of 1 m rotating at a slow speed

8.6.2 Case 2: One corner reflector located at a slant range of 2.5 m rotating at a slow speed

The resultant images shown in Fig. 8.11 were generated for one corner reflector target rotating at an angular velocity, Ω of 0.380 rad/s, at a radius of 0.5 m of the rotating platform's centre of rotation. The radar was placed at a slant range of 2.5 m away from the rotating platform. The radar system transmitted at a PRF of 20 Hz and an observation window of 0.8 s was considered, equivalent to 16 pulses, to limit the amount of range bin migration. The first observation from Fig. 8.11 is that the radar system was able to detect one corner reflector once again. The expected Doppler frequency was ± 3.2 Hz, however, from the image, the radar estimated a Doppler frequency between 1.245 Hz and 3.735 Hz at the locations with the highest signal intensities. The expected cross-range was 0.5 m, however, from the image the radar estimated a cross-range between 0.192 m and 0.578 m. The expected slant range was 2.5 m, however, the radar estimated a slant range between 2-3 at the locations on the Range-Doppler map with the highest signal intensities.

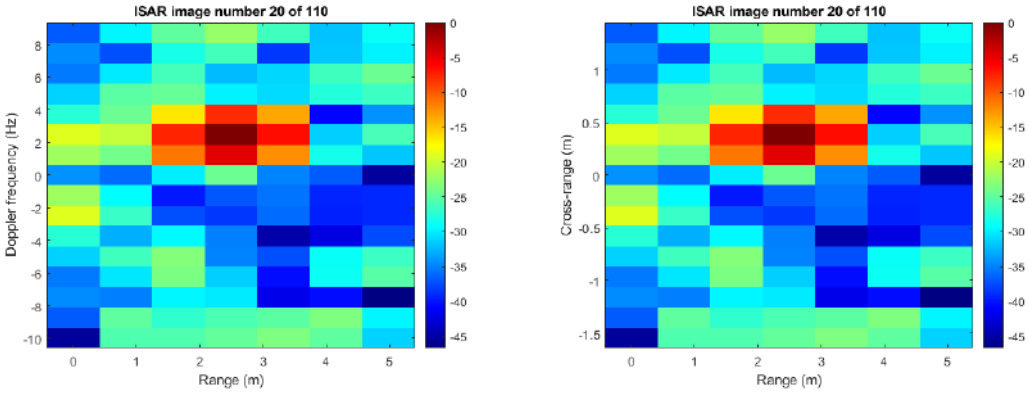

(a) Doppler frequency vs Range map (b) Cross-range vs Range map

Figure 8.11: Resultant ISAR images for two corner reflectors located at a slant range of 2.5 m rotating at a slow speed

8.6.3 Case 3: Two corner reflectors located at a slant range of 1 m rotating at a slow speed

The resultant images shown in Fig. 8.12 were generated for one corner reflector target rotating at an angular velocity, Ω of 0.380 rad/s, at a radius of 0.5 m of the rotating platform's centre of rotation. The radar was placed at a slant range of 1 m away from the rotating platform. The radar system transmitted at a PRF of 20 Hz and an observation window of 0.8 s was considered, equivalent to 16 pulses, to limit the amount of range bin migration. The first observation from Fig. 8.12 is that the radar system was able to detect two corner reflectors. The expected Doppler frequency was $\pm$3.2 Hz, however, from the image, the radar estimated a Doppler frequency between 1.245 Hz and 3.735 Hz at the locations with the highest signal intensities. The expected cross-range was 0.5 m, however, from the image, the radar estimated a cross-range between 0.192 m and 0.578 m. The expected slant range was 1 m, however, the radar estimated a slant range varying between 1-2 at the locations on the Range-Doppler map with the highest signal intensities.

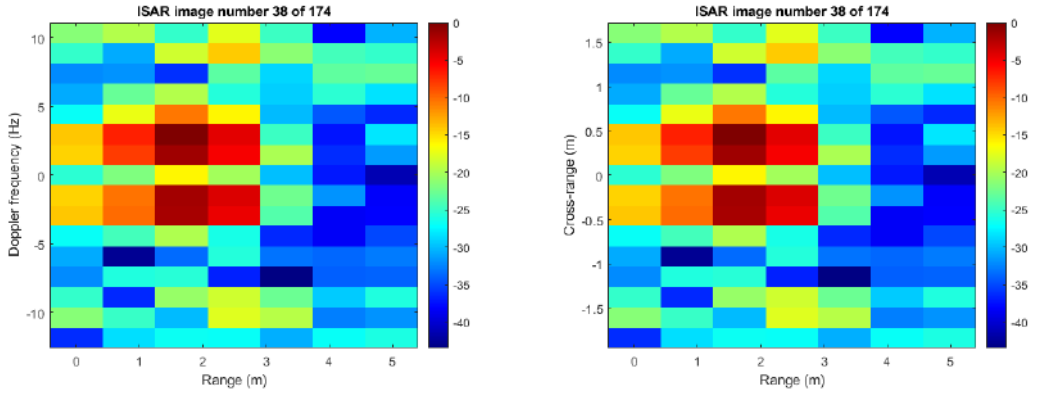

(a) Doppler frequency vs Range map

(b) Cross-range vs Range map

Figure 8.12: Resultant ISAR images for two corner reflectors located at a slant range of 1 m rotating at a slow speed

8.6.4 Case 4: Two corner reflectors located at a slant range of 2.5 m rotating at a slow speed

The resultant images shown in Fig. 8.13 were generated for one corner reflector target rotating at an angular velocity, Ω of 0.380 rad/s, at a radius of 0.5 m of the rotating platform centre of rotation. The radar was placed at a slant range of 2.5 m away from the rotating platform. The radar system transmitted at a PRF of 20 Hz and an observation window of 0.8 s was considered, equivalent to 16 pulses, to limit the amount of range bin migration. The first observation from Fig. 8.13 is that the radar system was able to detect two corner reflectors. The expected Doppler frequency was $\pm$3.2 Hz, however, from the image, the radar estimated a Doppler frequency between 2 Hz and 4 Hz at the locations with the highest signal intensities. The expected cross-range was 0.5 m, however, from the image, the radar estimated a cross-range centred on 0.5 m. The expected slant range was 2.5 m, however, the radar estimated a slant range varying between 2-4 at the locations on the Range-Doppler map with the highest signal intensities.

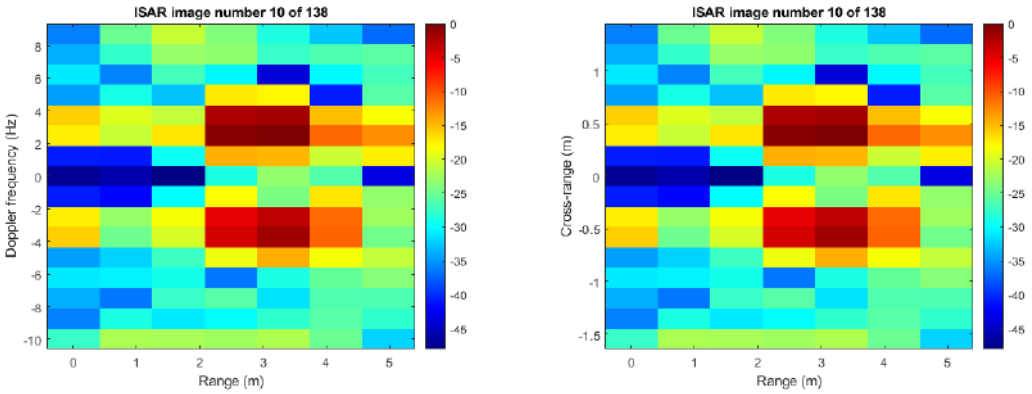

(a) Doppler frequency vs Range map

(b) Cross-range vs Range map

Figure 8.13: Resultant ISAR images for two corner reflectors located at a slant range of 2.5 m rotating at a slow speed

8.7 Conclusion

The aim of this phase of the project was to determine if it would be feasible to perform ISAR imaging with the MIT coffee can radar by developing a demonstration prototype. The requirements for the prototype were determined and design calculations were performed to determine the necessary radar specifications to utilise for ISAR imaging. Experiments were conducted with hand-made corner reflectors as targets and it was found that the radar system could be used to reconstruct images of target scenes with one and two corner reflectors. The radar performed poorly with regards to its resolution and accuracy in estimating the expected Doppler frequencies and slant range of the targets. However, the corner reflectors could clearly be observed in the ISAR images at the predicted slant-range and cross-range positions. It can be concluded, that it was feasible to utilise the MIT coffee can radar for educational ISAR imaging demonstrations.

Chapter 9

Conclusions

The aim of this project was to evaluate the effectiveness of the MIT coffee can radar as an educational tool. The methodology that was followed involved firstly executing tests on the radar system to determine whether it functioned correctly on a subsystem level. Secondly, indoor and outdoor experiments were performed to demonstrate the radar's capabilities to measure the range and the speed of human targets. Lastly, an investigation was conducted to determine whether the radar could be used for ISAR imaging by designing an ISAR imaging demonstration prototype. Throughout these three stages of the project, the overarching goal was always to extract the educational value of the radar system during each phase.

During the system testing phase, tests were conducted on the low frequency circuits and high-level concepts in electrical engineering governed the operation of those circuits, such as amplification, filtering, voltage regulation and Nyquist sampling theory. The 4th order low pass filtered out high frequency content in the IF signal producing a baseband signal that could be sampled by the sound card. The amplifier stage demonstrated the concept of amplification. The power supply circuit demonstrated the concept of voltage regulation. When developing the test procedures, the determination of the expected results were based on circuit theory, such as how the gain of the amplifier depended on the negative feedback loop resistance of the operational amplifier circuit. The characteristics of the amplifier's output signal was also influenced by the positive DC offset placed on its output that was added to the circuit.

After performing the test procedures, the results measured were not always exactly as expected. For example, when determining the frequency response of the low pass filter in the video amplifier circuit, a frequency roll-off of -80 dB/decade was expected, however a roll-off of -55 dB/decade was measured. This showed the reality of circuit design, that the actual behaviour of electronic circuits does not always match the expected designed behaviour. This is because real electronic circuits are not ideal and are also susceptible to component tolerances. The goal of practical-based education is to allow the theory that is learnt to be seen in practice and this was achieved during the radar integration tests. During these tests, it was observed how the different electronics and radio frequency subsystems of the radar worked together to achieve the different modes of operation of the radar system and contributed to the educational value of the radar.

During the indoor and outdoor experiments, applications of the radar system were demonstrated because the system was able to measure the range and speed of targets. These experiments provided a way to see how radar theory was being applied in practice. By operating the radar in CW mode and FMCW mode, it brought to life all the theories behind the operation of CW-Doppler and FMCW radars. These experiments also provided a way to see how changing the parameters of the radar affect its performance. During the ISAR imaging prototype design phase, a system design process was followed to develop a system to demonstrate ISAR imaging using the radar. The design process involved defining the requirements and performing design calculations based on the ISAR imaging theory and radar signal processing software design and development. The results of investigation determined that the radar could be used for ISAR imaging, demonstrating the educational value of the radar.

Chapter 10

Recommendations and future work

During the course of the project, observations were made as the MIT coffee can radar system was evaluated during the system testing phase, range and Doppler experiment phase and ISAR demonstration phase of the project. The following paragraphs explain the observations and recommendations and future work that can be done related to the radar masters programme at UCT.

During the outdoor experiments, it was observed that the functionality of the low frequency subsystem, specifically the modulator circuit of the radar system could be extended further. The current design of the modulator circuit involves making use of potentiometers to adjust waveform parameters such as the tuning voltage amplitude and period and requires making use of an oscilloscope to measure the output signal of the circuit. Therefore, if outdoor experiments are performed, it would be a challenge to adjust the tuning voltage parameters, such as increasing PRF for Doppler measurements because there would be no mechanism to provide feedback to the user that the radar has been set to the desired parameters. In the literature covered during the literature review, a common modification to the radar was the use of a microcontroller to digitally generate the required frequency modulating waveforms [7, 11, 34], and then converting the digital signal to an analogue signal, using an analogue to digital converter. That signal can then be utilised as the tuning voltage to the oscillator. This approach would also allow the radar system to use different frequency modulation waveforms, such as a sawtooth wave and a stepped frequency waveform. These modifications could be integrated as practical coursework in the Radar masters programme as embedded systems work related to radar systems.

The low frequency circuits on the circuit board were implemented using soldered through-hole components. Such circuits are commonly susceptible to variance in performance and producing noisy signals, possibly due to poor solder joints. Therefore, another recommendation would be to redesign the low frequency circuits using surface mount components. Third-party companies such as JLCPCB provide cost-effective printed circuit board (PCB) prototype fabrication services and require the circuit schematics and design files generated. JLCPCB's services have already been used at UCT before, such as in the project component of the 3rd year electrical engineering design principles course, presented in 2022, and it proved to be a pedagogical success. Performing these modifications to the circuit and fabricating new circuit boards could also be integrated into the Radar masters programme as a circuit design course component related to radar systems engineering.

Bibliography

[1] M. A. Richards, Ed., *Principles of Modern Radar: Basic principles*, ser. Radar, Sonar amp; Navigation. Institution of Engineering and Technology, 2010.

[2] V. C. Chen, *Inverse Synthetic Aperture Radar Imaging: Principles, Algorithms and Applications*, ser. Radar, Sonar amp; Navigation. Institution of Engineering and Technology, 2014. [Online]. Available: https://digital-library.theiet.org/content/books/ra/sbra504e

[3] uRAD, "Radar solutions." [Online]. Available: https://urad.es/en/productos/

[4] G. L. Charvat, A. J. Fenn, and B. T. Perry, "The MIT IAP Radar Course: Build a Small Radar System Capable of Sensing Range, Doppler, and Synthetic Aperture (SAR) Imaging*," *2012 IEEE Radar Conference*, 2012.

[5] G. L. Charvat, "MIT OCW: Build a Small Radar System Capable of Sensing Range, Doppler, and Synthetic Aperture (SAR) Imaging," 2011. [Online]. Available: https://ocw.mit.edu/courses/res-ll-003-build-a-small-radar-system-capable-of-sensing-range-doppler-and-synthetic-aperture-radar-imaging pages/projects/

[6] A. Forbes, "Radar detection of ground targets," 2018.

[7] S. G. Gutierrez, N. L. Bertolo, J. A. Areta, and D. E. Neuman, "Design of a low-cost continuous-wave Doppler RADAR operating at 2.4 GHz," in *2021 Argentine Conference on Electronics - Congreso Argentino de Electronica 2021, CAE 2021*. Institute of Electrical and Electronics Engineers Inc., mar 2021, pp. 19–24.

[8] R. Yannick Cabral Lopes Dias and T. Liu, "Designing, Measurement and Analysis of a Short Range FMCW Radar; Designing, Measurement and Analysis of a Short Range FMCW Radar," *2019 4th International Conference on Electromechanical Control Technology and Transportation (ICECTT)*, 2019.

[9] J. Carroll, G. Paparisto, and D. Vye, "The "coffee-can" radar redesigned as an inexpensive RF PCB [Application Notes]," *IEEE Microwave Magazine*, vol. 17, no. 10, pp. 62–74, oct 2016.

[10] O. Basarslan and E. Yaldiz, "Implementation of FMCW radar for training applications," in *2017 4th International Conference on Electrical and Electronics Engineering, ICEEE 2017*. Institute of Electrical and Electronics Engineers Inc., may 2017, pp. 304–308.

[11] S. Park, Y. Kim, K. Lee, A. H. Smith, J. E. Dietz, and E. T. Matson, "Accessible real-time surveillance radar system for object detection," *Sensors (Switzerland)*, vol. 20, no. 8, pp. 1–18, 2020.

[12] A. Zozaya and R. Bolaños, "Implementing the LFM-CW MIT radar at the ecuadorian space institute: Some results," *Journal of Aerospace Technology and Management*, vol. 12, no. 1, pp. 2–14, 2020.

[13] Y. Medina, M. Augusto, A. Navarro, S. M. Odiaga, H. Joussef, and M. Platriez, "Synthetic aperture radar (SAR) imaging based on low-cost FMCW radar for mini-UAVs," in *Proceedings of the 2016 IEEE ANDESCON, ANDESCON 2016*. Institute of Electrical and Electronics Engineers Inc., jan 2017.

[14] M. A. Jensen, D. V. Arnold, D. E. Crockett, M. A. . Jensen, and D. V. . Arnold, "System level microwave design: Radar-based laboratory projects System level microwave design: Radar-based laboratory projects," *IEEE Transactions on Education*, vol. 43, no. 4, 2000. [Online]. Available: https://scholarsarchive.byu.edu/facpub.586

[15] A. J. Camps, "A Radar Course at Undergraduate Level: An Approach to Systems Engineering," *IEEE Transactions on Education*, vol. 46, no. 4, pp. 497–501, nov 2003.

[16] J. P. Becker, "Using antenna arrays to motivate the study of sinusoids," *IEEE Transactions on Education*, vol. 53, no. 2, pp. 209–215, may 2010.

[17] R. F. Hollender and J. Becker, "Development of a Doppler radar experiment board for use in microwave circuits and electronics courses," *ASEE Annual Conference and Exposition, Conference Proceedings*, 2010.

[18] E. Aydin and N. Cagiltay, "A new RF and Microwave Engineering course enriched with advanced technologies," *Computer Applications in Engineering Education*, vol. 20, no. 4, pp. 634–645, dec 2012. [Online]. Available: https://onlinelibrary.wiley.com/doi/full/10.1002/cae.20432

[19] U. Hernandez-Jayo, J. M. Lopez-Garde, and J. E. Rodriguez-Seco, "Addressing electronic communications system learning through a radar-based active learning project," *IEEE Transactions on Education*, vol. 58, no. 4, pp. 269–275, nov 2015.

[20] B. T. Perry, T. Levy, P. Bell, S. Davis, K. Kolodziej, N. O'Donoughue, and J. S. Herd, "Low cost phased array radar for applications in engineering education," *IEEE International Symposium on Phased Array Systems and Technology*, pp. 416–420, 2013.

[21] F. Vincent, B. Mouton, E. Chaumette, C. Nouals, and O. Besson, "Synthetic aperture radar demonstration kit for signal processing education," *ICASSP, IEEE International Conference on Acoustics, Speech and Signal Processing - Proceedings*, vol. 3, 2007.

[22] Anteral, "Radar." [Online]. Available: https://anteral.com/radar/

[23] ——, "uRAD Universal Radar at 24 GHz for Arduino," 2022. [Online]. Available: https://urad.es/wp-content/descargables/uRAD%20-%20Datasheet%20-%20Arduino%20v1.1%20-%20EN.pdf

[24] ——, "uRAD Universal Radar at 24 GHz for Raspberry Pi," 2022. [Online]. Available: https://urad.es/wp-content/descargables/uRAD%20-%20Datasheet%20-%20RaspberryPi%20v1.2%20-%20EN.pdf

[25] ——, "uRAD Universal Radar at 24 GHz for USB," 2022. [Online]. Available: https://urad.es/wp-content/descargables/uRAD%20-%20Datasheet%20-%20USB%20v1.2%20-%20EN.pdf

[26] ——, "urad industrial v1.0." [Online]. Available: https://urad.es/wp-content/descargables/uRAD%20-%20Datasheet%20-%20Industrial%20v1.0%20-%20EN.pdf

[27] ——, "urad automotive v1.0." [Online]. Available: https://urad.es/wp-content/descargables/uRAD%20-%20Datasheet%20-%20Automotive%20v1.0%20-%20EN.pdf

[28] TDSR, "P440 UWB Module," 2020. [Online]. Available: http://tdsr-uwb.com/wp-content/uploads/2021/03/320-0317G-P440-Data-Sheet-User-Guide.pdf

[29] Acconeer, "Entry module EVK hardware user guide - XE132," 2021. [Online]. Available: https://developer.acconeer.com/download/xe132-user-guide-pdf/

[30] Quonset, "QM-RDK Radar Demonstration Kit - User manual," 2016. [Online]. Available: https://www.quonsetmicrowave.com/v/vspfiles/Manuals/QM-RDKIT/QM-RDK%20User%20Manual%20REV%201.2.0.pdf

[31] Pasternack, "Radar Development Kit Technical Datasheet - PEM11000-KIT," 2016. [Online]. Available: https://www.pasternack.com/images/ProductPDF/PEM11000-KIT.pdf

[32] Quonset, "Qm-rdkit radar demonstration kit." [Online]. Available: http://www.quonsetmicrowave.com/QM-RDKIT-p/qm-rdkit.htm

[33] Pasternack, "2.4 ghz to 2.5 ghz ism band radar demonstration kit." [Online]. Available: https://www.pasternack.com/2.5-ghz-radar-development-system-pem11000-kit-p.aspx

[34] V. Ferrara, F. Troiani, F. Frezza, F. Mangini, L. Pajewski, P. Simeoni, and N. Tedeschi, "Design and Realization of a cheap Ground Penetrating Radar Prototype @ 2.45 GHz," *2016 10th European Conference on Antennas and Propagation, EuCAP 2016*, pp. 6–9, 2016.

[35] S. Park, S. Shin, Y. Kim, E. T. Matson, K. Lee, P. J. Kolodzy, J. C. Slater, M. Scherreik, M. Sam, J. C. Gallagher, B. R. Fox, and M. Hopmeier, "Combination of radar and audio sensors for identification of rotor-type Unmanned Aerial Vehicles (UAVs)," *2015 IEEE SENSORS - Proceedings*, dec 2015.

Appendix A

Code

The GitHub repository containing all code that was written for the ISAR demonstrator can be accessed at: `https://github.com/samuelmbiya/Evaluating-the-MIT-S-band-radar-as-an-educational-tool.git`

Appendix B

ZX95-2536C+ VCO datasheet

*Performance Data & Curves**

ZX95-2536C+

V TUNE	TUNE SENS (MHz/V)	FREQUENCY (MHz)			POWER OUTPUT (dBm)			Icc (mA)	HARMONICS (dBc)			FREQ. PUSH (MHz/V)	FREQ. PULL (MHz)	PHASE NOISE (dBc/Hz) at offsets				FREQ OFFSET (KHz)	PHASE NOISE at 2432 MHz (dBc/Hz)
		-55°C	+25°C	+85°C	-55°C	+25°C	+85°C		F2	F3	F4			1kHz	10kHz	100kHz	1MHz		
0.00	81.90	2267.6	2257.4	2249.2	5.54	5.14	4.51	36.63	-21.7	-19.0	-36.6	2.44	3.28	-77.7	-104.8	-127.5	-147.0	1.0	-75.73
0.50	74.61	2306.7	2297.3	2289.5	5.76	5.23	4.62	37.11	-30.5	-20.4	-35.5	1.96	0.44	-76.2	-105.1	-128.0	-147.9	2.0	-84.74
0.75	73.96	2325.2	2315.9	2308.2	5.87	5.27	4.67	37.29	-36.1	-21.6	-35.4	1.65	1.90	-76.2	-105.7	-128.6	-148.2	3.5	-93.54
1.00	73.76	2344.0	2334.4	2326.4	5.86	5.32	4.77	37.45	-32.0	-22.3	-36.4	1.49	2.67	-75.5	-105.6	-128.2	-147.6	6.0	-99.82
1.25	73.75	2362.7	2352.9	2344.6	5.86	5.38	4.83	37.57	-28.6	-22.4	-37.9	1.42	2.27	-77.8	-105.5	-128.7	-148.3	8.5	-103.77
1.50	74.01	2381.6	2371.3	2362.6	5.87	5.43	4.92	37.67	-25.6	-22.5	-39.9	1.37	1.25	-77.6	-105.5	-128.7	-148.4	10.0	-105.41
1.75	74.71	2400.7	2389.8	2380.6	5.87	5.52	5.03	37.73	-23.5	-23.3	-41.2	1.38	1.27	-76.5	-105.6	-128.9	-148.5	20.8	-113.60
2.00	74.15	2419.7	2408.5	2398.9	5.89	5.58	5.12	37.80	-22.2	-23.5	-44.0	1.41	2.83	-77.1	-105.6	-128.9	-148.4	35.5	-118.96
2.25	73.21	2438.5	2427.0	2417.2	5.90	5.62	5.21	37.87	-20.8	-23.5	-43.4	1.51	2.86	-76.1	-105.9	-128.8	-148.6	60.7	-124.10
2.50	71.91	2456.9	2445.3	2435.4	5.92	5.69	5.28	37.92	-20.0	-23.9	-43.5	1.75	1.53	-76.5	-105.6	-128.7	-148.8	85.2	-127.31
2.75	70.82	2475.0	2463.3	2453.3	6.00	5.73	5.33	37.95	-19.5	-24.7	-43.9	2.12	1.51	-75.3	-104.9	-128.6	-148.1	100.0	-128.68
3.00	68.45	2492.6	2481.0	2471.1	6.01	5.80	5.40	37.97	-18.5	-25.3	-44.9	2.58	3.12	-76.0	-104.4	-128.3	-148.6	142.9	-131.46
3.25	65.44	2509.4	2498.1	2488.3	6.09	5.87	5.44	37.99	-17.9	-25.3	-45.0	3.09	2.95	-74.7	-104.6	-128.1	-148.7	167.8	-133.29
3.50	61.36	2525.2	2514.5	2504.9	6.16	5.91	5.54	38.02	-17.3	-27.7	-46.3	3.65	1.69	-76.0	-104.2	-128.2	-148.0	200.6	-134.52
3.75	57.60	2540.3	2529.8	2520.7	6.18	5.97	5.58	38.06	-16.8	-27.5	-47.3	4.08	1.15	-75.5	-103.9	-128.4	-147.5	281.6	-137.84
4.00	53.56	2554.4	2544.2	2535.4	6.26	6.01	5.66	38.06	-16.3	-30.1	-48.7	4.52	2.96	-77.2	-103.4	-128.0	-147.9	330.7	-138.85
4.25	50.01	2567.6	2557.6	2549.0	6.30	6.08	5.70	38.06	-16.1	-31.4	-49.8	4.84	3.53	-77.3	-103.2	-127.7	-147.8	464.2	-141.63
4.50	45.62	2579.9	2570.1	2561.7	6.33	6.10	5.76	38.05	-15.6	-33.0	-49.1	5.01	3.11	-77.3	-103.3	-127.8	-148.3	554.9	-143.78
4.75	41.10	2591.0	2581.5	2573.3	6.38	6.15	5.79	38.05	-15.5	-37.8	-50.1	5.07	2.11	-76.0	-103.0	-127.6	-148.2	914.6	-147.64
5.00	36.26	2601.0	2591.8	2583.8	6.40	6.17	5.83	38.06	-15.2	-35.9	-51.1	4.89	0.87	-75.8	-103.4	-128.1	-148.4	1000.0	-148.33

*at 25°C unless mentioned otherwise

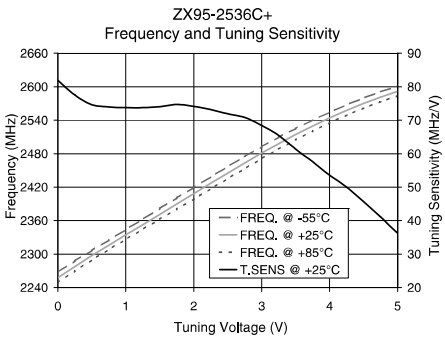

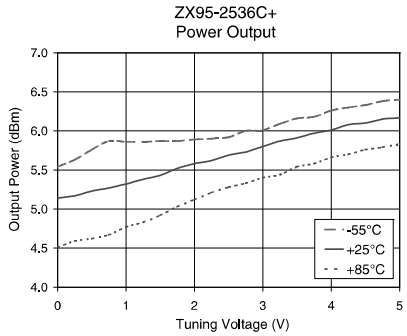

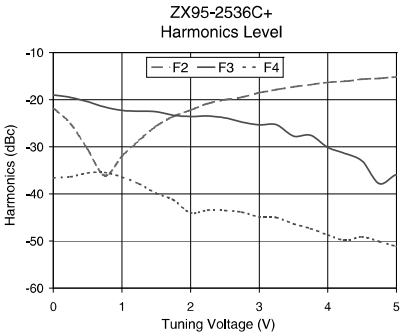

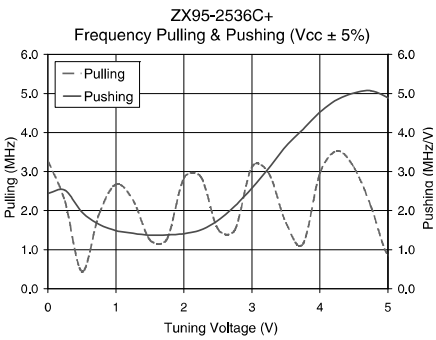

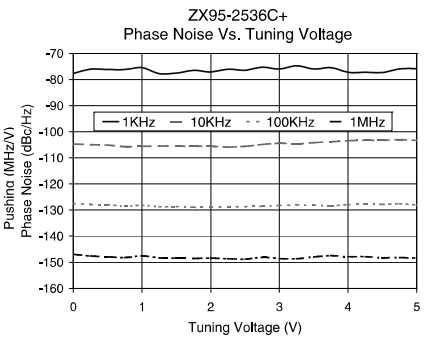

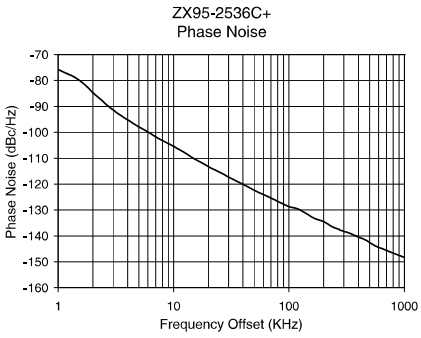

Appendix C

Complete radar system initial testing results

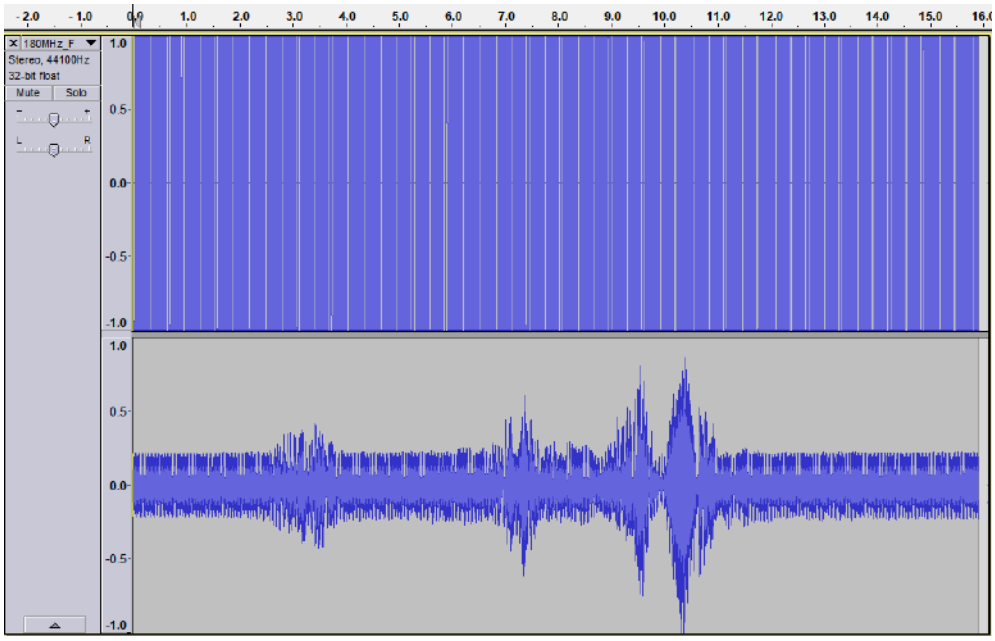

Figure C.1: An image showing a full view of the sampled output signal from the low frequency subsystem in CW mode using the Audacity digital audio software. The left channel (top) shows an enabled sync pulse and the right channel (bottom) shows the baseband signal received

Appendix D

Outdoor range experiment setup and results

(a) Image 1 (b) Image 2

Figure D.1: Images showing the actual set up of the outdoor experiments

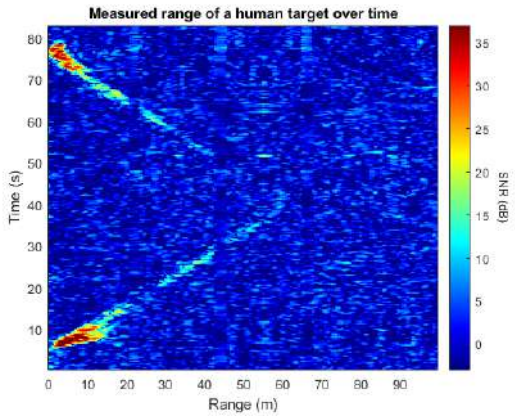

Figure D.2: A plot showing the range of a human target over time while walking towards the 50 m rugby line and back towards the radar system (PRI = 260 ms)

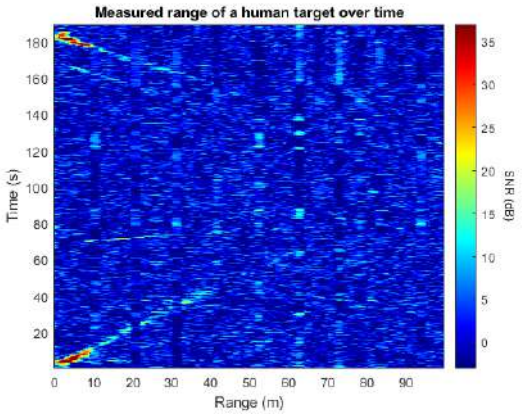

Figure D.3: A plot showing the range of a human target over time while walking towards the 100 m rugby line and back towards the radar system (PRI = 60 ms)

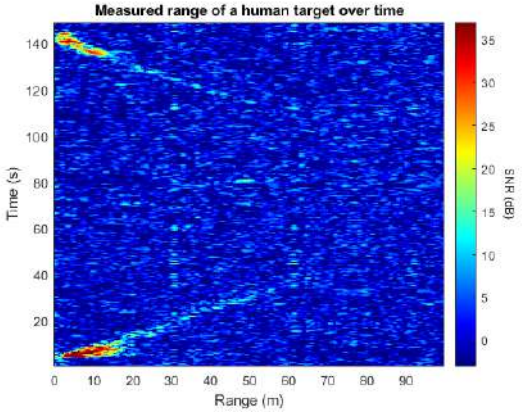

Figure D.4: A plot showing the range of a human target over time while walking towards the 100 m rugby line and back towards the radar system (PRI = 370 ms)

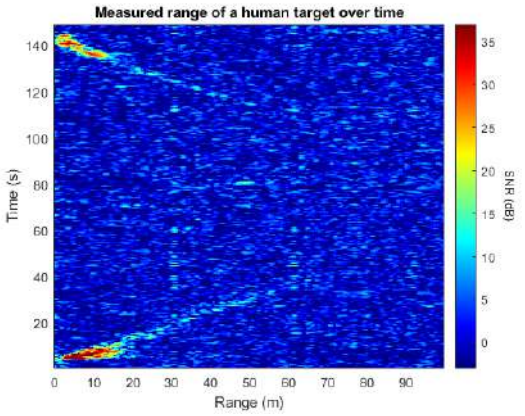

Figure D.5: A plot showing the range of a human target over time while walking towards the 100 m rugby line and back towards the radar system (PRI = 370 ms)

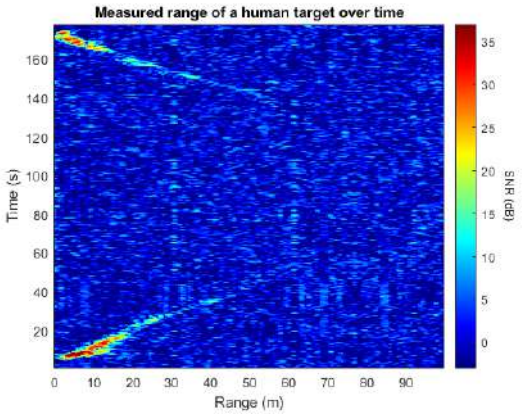

Figure D.6: A plot showing the range of a human target over time while walking towards the 100 m rugby line and back towards the radar system (PRI = 370 ms)

Appendix E

ISAR imaging results

E.1 Case 1: One corner reflector located at a slant range of 1 m rotating at a fast speed

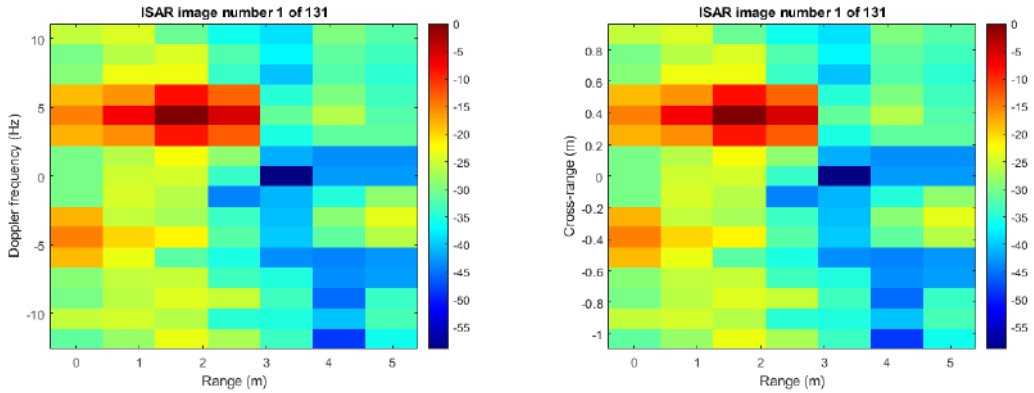

(a) Doppler vs Range map (b) Cross-range vs Range map

Figure E.1: Resultant ISAR images for one corner reflector located at a slant range of 1 m rotating at a fast speed

E.2 Case 3: Two corner reflectors located at a slant range of 1 m rotating at a fast speed

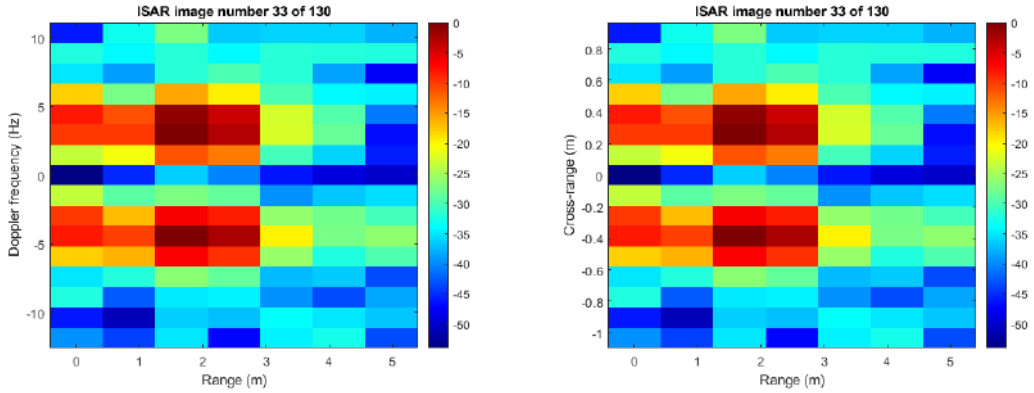

(a) Doppler vs Range map (b) Cross-range vs Range map

Figure E.2: Resultant ISAR images for two corner reflectors located at a slant range of 1 m rotating at a fast speed